Volcaniclastic deposits and sedimentation processes around volcanic ocean islands: the central Azores

Full title: Volcaniclastic deposits and sedimentation processes around volcanic ocean islands: the central Azores

Abbreviated title: Volcaniclastic deposits in the central Azores

Yu-Chun Chang[1, *], Neil C. Mitchell[1], Thor H. Hansteen[2], Julie C. Schindlbeck-Belo[2], Armin Freundt[2]

[1]Department of Earth and Environmental Sciences, University of Manchester, Williamson Building, Oxford Road, Manchester M13 9PL, UK.
[2] GEOMAR, Helmholtz Centre for Ocean Research Kiel, Wischhofstrasse 1–3, Kiel 24148, Germany

*Correspondence to: Yu-Chun Chang (yu-chun.chang@manchester.ac.uk)

This is the green open-access version of the above-titled article accepted for publication on 26 August 2021, in "Volcanic Processes in the Sedimentary Record: When Volcanoes Meet the Environment" (ed by: A. Di Capua, R. De Rosa, G. Kereszturi, E. Le Pera, M. Rosi and S.F.L. Watt), Geol. Soc. Lond. Spec. Publ. (doi: 10.1144/SP520-2021-62; *link to access the published article:* https://doi.org/10.1144/SP520-2021-62).

Abstract

Geological histories of volcanic ocean islands can be revealed by the sediments shed by them. Hence there is an interest in studying cores of volcaniclastic sediments that are particularly preserved in the many flat-floored basins lying close to the Azores islands. We analyse four gravity cores collected around the central group of the islands. Three sedimentary facies (F1-F2a, F2b) are recognized based on visual core logging, particle morphometric and geochemical analyses. F1 is clay-rich hemipelagite comprising homogeneous mud with mottled structures from bioturbation. F2a and F2b are both clay-poor volcaniclastic deposits, which are carbonate-rich and carbonate-poor, respectively. More biogenic carbonate in F2a reflects the incorporation of unconsolidated calcareous material from island shelves or bioturbation. Within F2a and F2b we identify deposits emplaced by pyroclastic fallout, primary or secondary turbidity currents by combining multiple information from lithological composition, sedimentary structures, chemical composition of volcanic glass shards and morphometric characteristics of volcanic particles. Primary volcaniclastic sediments were found in all four cores, echoing activity known to have occurred up to historical times on the adjacent islands. These preliminary results suggest that greater details of geological events could be inferred for other volcanic islands by adopting a similar approach to core analysis.

Keywords: volcaniclastic facies, volcanic islands, volcanic hazard, geohazard history, grain-shape analysis

Large volumes of volcaniclastic sedimentary material are denuded from volcanic ocean islands and transferred to their surrounding seafloor (Menard 1983), so scientific drilling and shallow coring can be used to determine how the transfer of volcaniclastic sediments has varied over time. At more distal sites, turbidity currents associated with mass wasting of islands are typically less erosive, so more dateable hemipelagic sediments between turbidites can be preserved. However, only turbidity currents produced by large events such as flank collapses are likely to reach distal sites (Hunt *et al.* 2011; 2013). More proximal sites, in contrast, have a good chance of recording smaller volcanic eruption and collapse events (e.g., Wall-Palmer *et al.* 2014). Examples of sampling sites close to oceanic islands include those of Ocean Drilling Program (ODP) Leg 157 offshore Gran Canaria (Carey *et al.* 1998; Schmincke and Sumita 1998), shallow coring offshore Reunion Island (Ollier *et al.* 1998; Saint-Ange *et al.* 2013), and Cape Verde islands (Eisele *et al.* 2015a, b). Intensive sampling near to arc volcanic islands has been carried out near Montserrat, including during International Ocean Discovery Program (IODP) Expedition 340 (Le Friant *et al.* 2015) and with extensive shallow coring (Trofimovs *et al.* 2006; Trofimovs *et al.* 2013; Cassidy *et al.* 2014). Proximal sites tend to have well-preserved turbidite sequences, although scouring by the turbidity currents can erode their sedimentary substrates as well (e.g., Trofimovs *et al.* 2006; Solaro *et al.* 2020). The Montserrat cores in particular reveal how particles in pyroclastic flows are separated when they enter the ocean, with larger clasts rapidly deposited, leaving the finer particles to travel on as turbidity currents (Trofimovs *et al.* 2006). The IODP core results suggest evidence for seabed failure caused by loading by debris avalanche material (Le Friant et al., 2015). The many flat-floored basins lying within 10–30 km of the Azores islands are potential proximal sediment traps as turbidity currents from the island slopes became depositional upon

transformation to subcritical flow (e.g., van Andel and Komar 1969). These deposits can reveal how the sequence, frequency and style of mass-transport events on and around the islands have varied over time. They should also reveal if and how they differ from the more proximal sampling records obtained at other islands.

Volcaniclastic deposits can be sub-divided into primary and secondary deposits (Fisher 1961). Primary submarine volcaniclastic deposits are directly derived from volcanic activity, such as ash fallout from eruption columns (e.g., Bonadonna *et al.* 2002), subaqueously fragmenting lava flows from effusive vents (e.g., Cappello *et al.* 2015), and pyroclastic flows produced by collapsing eruption columns and domes entering the sea (e.g., Calder *et al.* 1999). Alongside those, primary deposits also include syn-eruptive deposits whose mode of transport may have included non-eruptive mechanisms, but where the clasts are a product of eruptive activity and where transport occurs without an intervening stage of deposition and remobilisation. For example, the immediate mixing of pyroclastic material with water/ice can generate lahars reaching the sea (e.g., Cronin *et al.* 1997). Secondary deposits may be indirectly associated with eruptive activity, but most events are unrelated to volcanic activity. Massive landslides can potentially arise from the instability of steep slopes of volcanic islands coupled with various triggers (Lee *et al.* 1994; Keating and McGuire 2000). Secondary volcaniclastic deposits unrelated to volcanic activity can also be caused by a wide range of reworking processes, for instance, sediment resuspension during tropical hurricanes or storms (Dengler *et al.* 1984), submarine slope collapses due to over-steepening of unconsolidated volcanic materials (Fornari *et al.* 1979) or suspension of particles by coastal waves (Quartau *et al.* 2012; Zhao *et al.* 2019) or subaerial erosion (Louvat and Allègre 1998).

Biogenic production in the shallow waters of the Azores Islands has made carbonate a common non-volcaniclastic component of their shelf deposits (Quartau *et al.* 2012; 2015; Ávila *et al.* 2015; Wisshak *et al.* 2015), which is potentially exported to the basins, where it could be a useful tracer of shelf or upper slope origins. The relative amounts of different types of sediment should vary between islands, e.g., due to different dominant eruption styles (explosive versus effusive) or size and structure of shelves. Biogenic production rates vary with food sources, water clarity and other factors (Wisshak *et al.* 2015). Coastal and subaerial erosion rates vary with wave, wind and precipitation conditions, even around individual islands due to shadowing (Mitchell *et al.* 2003).

The chemical compositions of volcanic fragments (typically of glass shards) in volcaniclastic deposits provide clues to their emplacement process and origin. In many instances, a deposit with a tight cluster of geochemical compositions has been interpreted as indicating a single volcanic event and thus a primary deposits (e.g., Stokes and Lowe 1988; Stokes *et al.* 1992; Lowe *et al.* 2017), although secondary volcaniclastic deposits may also have homogeneous shard compositions if those shards were derived from the remobilization of shelf-deposited tephra of unique magmatic systems largely stored on the shelf (Schneider *et al.* 2001). A large geochemical compositional variation instead likely results from reworking of material from different volcanic source deposits. However, in some cases, physically different volcanic sources contributing to deposits can differ only subtly geochemically (Boygle 1999; Schneider *et al.* 2001; Gudmundsdóttir *et al.* 2011; Schindlbeck *et al.* 2013), making interpretation of resedimented deposits based on geochemistry alone difficult. Such issues may also limit the use of chemical proxies in isolation to determine the origins of volcaniclastic deposits (e.g., Kratzmann *et al.* 2009; Christopher *et al.* 2014). Analyses of glass

geochemistry integrated with other information are therefore required for accurate and consistent identification of eruption sources.

We seek to reveal the main emplacement mechanism of volcaniclastic deposits on the basin floor of the central Azores by identifying different types of volcaniclastic deposits. The work aims to answer: are most of those deposits derived directly from volcanic eruptions (primary volcaniclastic deposits) or derived from reworked deposits or submarine slope failure (secondary volcaniclastic deposits)? The volcaniclastic bed thicknesses found here also pose the question of how they compare with other islands with different geological histories, as cores typically only sample a limited amount of sediment, both spatially and in terms of age extent, and classification of bed types varies between investigations. Comparing the results of coring in similar relatively proximal locations at other oceanic islands with similar hot-spot origin could reveal interesting variances that reflect differences in style of volcanism, seismicity and turbidite emplacement mechanisms. This article describes sediments in four gravity cores of 13 m total length by integrating visual observations, geochemical measurements and grain-shape morphometric analyses. Multiple types of sediment characteristics are used to classify the sediments.

Geological setting

The central Azores group of Terceira, São Jorge, Faial, Pico and Graciosa islands have grown during at least the Quaternary (Féraud *et al.* 1980) close to the slow spreading Mid-Atlantic Ridge (Fig. 1). The crust underlying them is thickened and forms a broad oceanic plateau, created by excess volcanism on a plate or at a plate boundary that has been slowly moving over a mantle hotspot or other source of excess mantle melting (White *et al.* 1976; Bonatti 1990; Gente *et al.* 2003; Vogt and Jung 2004). Several of the islands are WNW–ESE elongated (Fig. 1). Volcanic vents tend to form two distinct geochemical groups with different alignments (N150˚E and N110˚E–N120˚E), possibly a result of regional trans-tensional deformation (Lourenço *et al.* 1998; Miranda *et al.* 2015). Eruptive styles have ranged from effusive Hawaiian and mildly explosive Strombolian through phreatomagmatic to Plinian and ignimbrite eruptions associated with caldera formation (Machado 1959; Weston 1964; Madeira 1998; Cole *et al.* 2001; Calvert *et al.* 2006; Pimentel 2007; Larrea *et al.* 2014; Sibrant *et al.* 2014). Effusive eruptions producing lava flows have usually been associated with the fissure zones. Besides on-going seismicity (Miranda *et al.* 2015), fault offsets of Holocene lava flows and cinder cones are evidence of on-going tectonic activity (Madeira and Brum da Silveira 2003). Volcanic activity, earthquakes and storm-related activity potentially all cause episodic shedding of sediments from the islands.

Volcanoes in the central Azores have been historically active with events occurring since island settlement (Fig. 1; Gaspar *et al.* 2015). Young volcanic products can be found, for example, on Faial as historical lava flows and the <10 ka Capelo volcanic complex in the west of the island (Madeira 1998; Madeira and Brum da Silveira 2003). The rest of Faial is widely blanketed by volcanic deposits including ignimbrites, which were emplaced in a 1000 yBP explosive eruption of Caldeira Volcano (Pacheco 2002;

Pimentel *et al.* 2015). The whole of Pico Island is generally young and has continued growing over the Holocene (Woodhall 1974). The latest stages of basaltic lava flows originated from vents along the Fissural System in the middle of Pico Island and from Pico Mountain stratovolcano in the west (e.g., Forjaz 1968; Woodhall 1974; Zbyszewski *et al.* 1974; Madeira 1998; Nunes 1999). On São Jorge, the Young Volcanic Complex (<0.1 Ma) was unconformably deposited on both intermediate and old volcanic complexes in the centre of the island (Hildenbrand *et al.* 2008; Marques *et al.* 2018). On Terceira, major volcanic activity and the widespread ignimbrite were associated with the latest stages of growth of the west of the island since 23 ka (Self 1976). Santa Bárbara volcano, Pico Alto Volcano and the fissure zone crossing the island still show signs of activity (Self 1976; Féraud *et al.* 1980; Calvert *et al.* 2006; Gertisser *et al.* 2010).

Tall sea cliffs in the Azores indicate that coastal erosion also supplies terrigenous material, either onto shelves during current sea-level high-stand conditions or onto the submarine slopes by shelf spill-over. Zhao *et al.* (2019) documented the rapid erosion of the Capelinhos Cone since it was created by the eruption in 1957 (coastline initially retreating 164 m/y though with rate quickly declining after the eruption to 2 m/y). Zhao *et al.* (2020) used dated Holocene lava deltas and evidence of their previous extents underwater to work out retreat rates of 0.08 to 12.5 m/y at those deltas. Using a geochemical method, Louvat and Allègre (1998) inferred chemical denudation rates of 170–500 g/m^2/y and mechanical denudation rates of 26–50 g/m^2/y for Sao Miguel Island. These rates approximate to 0.06–0.18 m/y and 0.009–0.018 m/y when divided by a typical rock density of 2.7 g/m^3.

Production rates of carbonates on shelves are poorly known though artificial hardground experiments of Wisshak *et al.* (2010; 2015) southeast of Faial found rates

as high as ~631 g/m^2/y (i.e., ~0.225 m/y) at 60 m depth. Such high rates are typical of carbonate production, which varies strongly with timescale of measurement, tending to be higher when measured over short timescales (Schlager 2000), so these values overestimate the production rates on ky-timescales. Nevertheless, carbonate production on shelves, along with material from subaerial and coastal erosion, probably provides significant amounts of sediment to the shelves and slopes that may end up being deposited in the basins around the Azores Islands. Indeed, abundant landslide scars in the upper slopes of the islands (Fig. 1b; Mitchell *et al.* 2008; Quartau *et al.* 2010; Chang *et al.* 2019) and sediment waves on their lower flanks (Fig. 1b) are evidence for frequent slope failures and transport by sedimentary flows (Casalbore *et al.* 2020).

Materials and methods

The four gravity cores described here were collected around the central Azores islands (Fig. 1) during RV *Meteor* cruise M141/1 in 2017 (Hansteen *et al.* 2017) and are curated in the core repository at the GEOMAR-Helmholtz Centre for Ocean Research Kiel, Germany. Sampling points marked by types of analysis are located in Fig. 2. Samples are identified by core number and depth (e.g., 1226-90 represents the deposits of core 1226 at 90 cm below the seafloor).

Visual core descriptions and sample selection

Each core was photographed and inspected visually to produce sedimentary logs summarizing grain size changes, sedimentary structures and tephra-rich beds (Fig. 2). On the basis of those observations, 66 samples were taken for detailed microscope analysis, 52 for electron microprobe (EMP) analysis, 28 for grain-shape morphometric analyses, 14 for X-ray diffraction (XRD) analysis and 35 for total organic carbon/total nitrogen analysis (TOC/TN) and 23 for carbon isotope analysis ($\delta^{13}C$).

Volcanic glass geochemical analysis

Major element concentrations of volcanic glass shards were obtained by JEOL JXA 8200 wavelength dispersive electron microprobe (EMP) at GEOMAR Helmholtz Centre for Ocean Research, Kiel using procedures of Kutterolf *et al.* (2011). The size fraction 63–125 μm was extracted by wet-sieving. Glass shards were then selected and embedded in epoxy resin for analysis using a 15-kV accelerating voltage and 6 nA beam current at a defocused beam diameter of 5 μm. Lipari obsidian (peralkaline rhyolite; Hunt and Hill, 2001) and Smithsonian basalt VGA-99 (USNM 113498/1; Jarosewich 2002) were used as standards. In each sample, 60 individual glass shards were analysed except in very shard-poor samples (<10 vol%), where all visible glass shards were measured. Every sixty glass shard measurements were bracketed by four standard

measurements (two of each standard). Results with total oxides <95 wt% and accidental shots on minerals were excluded. Measured major element concentrations of standard materials deviate by <0.5% from the expected values. All measured values were normalised to 100 wt% to eliminate the effects of varied post-depositional hydration and minor deviations of electron beam focus.

Morphometric analyses of volcanic grains

The volcanic grain shape characterization used in this study was based on the work of Cassidy *et al.* (2014) with adjustments as follows. Volcanic grains were first manually separated (not sieved) from samples chosen from volcaniclastic-rich deposits, with carbonate-free grains selected (samples were not acid leached). The grains such as those in Figs. 5a–5d were photographed under a high magnification stereo microscope with white paper as background. Image spatial calibration, transformation and morphometric measurements were carried out with ImageJ software (Rasband WS, 1997–2012, https://imagej.nih.gov/ij) as also used by Cassidy *et al.* (2014). We measured cross-sectional area, aspect ratio and perimeter length of 30 to 60 grains per sample until graphs of the measured characteristics no longer changed with further measurements. Cross-sectional area was calculated from the sum of dark image pixels for each grain. Aspect ratio was calculated from the ratio of long axis to short axis. Perimeter lengths were converted to normalised perimeter lengths (NPLs) by dividing by the circumference of a circle of equivalent cross-sectional area in order to remove the effect of particle size. The characteristic length scale of each particle, representing its grain size, was calculated from square root of grain area and converted to the phi scale.

Bulk mineral assemblage analysis

Bulk sediment mineralogy was determined by X-ray powder diffraction (XRD) analysis. Samples were prepared following the methods of Charlier *et al.* (2006). Approximately 50 mg samples were powdered and analysed by Bruker D8 Advance diffractometer at the University of Manchester. A voltage of 40 kV and a tube current of 40 mA were used to produce CuKα1X-rays at a wavelength of 1.5406Å. Scanning range of the detector was set from 5–70° (2θ) with a step size of 0.02° and 2s per count. Diffraction angle peaks were evaluated with EVA version 5, with a mineral database originating from the International Centre for Diffraction Data (ICDD). Bulk mineralogy fractions were semi-quantitatively estimated using peak-area measurements with an analytical error of 0.5% (e.g., Schultz 1964).

Organic carbon and nitrogen and carbon isotope analyses

TOC was measured to assess potential organic carbon preservation and whether organic contents would help discriminate different types of sedimentary flow deposits. TOC/TN ratios and $\delta^{13}C$ were measured to provide information on carbon sources, in particular, algae and land plant sources (Meyers 1994). The sediment samples were first powdered and then separated into acid-untreated and acid-treated groups before measurements in multipurpose mass spectrometers at the University of Liverpool. Total organic carbon and organic carbon isotopes were measured on a subset of samples treated with 10% HCl. Total nitrogen was measured on a subset of samples without that HCl treatment. Standard samples were measured for every ten measurements. The operational detection limit of TOC was quoted as 0.1 wt%, although systematic differences in TOC between F2a and F2b suggests the detection limit may have reached closer to 0.05 wt% in practice. The average precision of $\delta^{13}C$ from repeated analyses is 0.2‰.

Discriminating pyroclastic fallout, primary turbidite and secondary turbidite

Emplacement mechanisms and origins (i.e., pyroclastic fallout and primary and secondary volcaniclastic turbidite) were determined by assessing all the information available from depositional structures, chemical compositions of volcanic glass shards and morphometric parameters of volcanic grains (Fig.2).

Bed colour, lithological composition, tractional structures and sharp bed contacts allowed the identification of volcaniclastic-rich beds. Laminated bedding, erosive bases and appearance of shelf-derived carbonate fragments indicate emplacement by sediment flows (cf. Bouma 1962; Stow and Piper 1984; Talling *et al.* 2012). Homogeneous volcanic glass compositions probably originate from single eruptions, hence deposits with such compositional homogeneity also conforming to the above features were interpreted as primary turbidites or, if reasonably well sorted and without indication of horizontal transport (traction features), as pyroclastic fallout. Although fallout deposits can share some sedimentary features with primary volcaniclastic turbidites, such as normal grading and sharp basal boundaries (e.g., Sigurdsson *et al.* 2000; Carey and Schneider 2011) and homogeneous chemical compositions, the high angularities (from both mean and standard deviation of NPL) are also helpful to distinguish them.

Heterogeneous geochemical compositions in sediment flow deposits instead reflect the mixing of particles from multiple sources, hence these are identified as secondary turbidites. However, interpretation of compositional homogeneity needs to consider possible complications. Erupted magmas can be compositionally zoned, in which case observed compositions are genetically related although possibly in a complex fashion (e.g., Sigurdsson and Sparks 1981; Freundt and Schmincke 1995). Conduit erosion, pyroclastic flows or edifice collapses can also entrain material from previous eruptions of genetically related magmas but possibly also enhance the occurrence of lithic

286 particles. On the other hand, an ocean island volcano may evolve either by repeatedly
287 erupting the same magma compositions over time or by gradually developing more
288 evolved compositions over time so that secondary turbidites originating by multi-stage
289 slope failures can have glass compositions that are homogeneous or follow a genetic
290 trend (Schneider *et al.* 2001; Hunt *et al.* 2011).

291 Although particles transported long distances by sediment flows are expected to
292 become less angular (Manga *et al.* 2011), those of primary volcaniclastic turbidites
293 transported short distances may remain sub-angular and maintain juvenile textures
294 (e.g., Sigurdsson *et al.* 1980; Houghton and Landis 1989), so they can be difficult to
295 distinguish from fallout by morphometric data alone. Moreover, intense post-
296 depositional bioturbation can mix sediments at the tops and bottoms of beds, which can
297 undermine the suggested typical characteristics of different volcaniclastic deposits. The
298 complexity of discrimination highlights that multiple types of parameters are needed to
299 interpret emplacement process and origins of volcaniclastic grains.

300 Total organic carbon contents were not used as criteria for assigning beds to fallout,
301 primary or secondary volcaniclastic deposits. Nevertheless, they were found to be
302 supportive as some deposits with extremely low TOC are easily explained by rapid
303 deposition of carbon-poor materials, as expected for primary volcaniclastic deposits.

Results

Three sedimentary facies (F1, F2a and F2b) were distinguished by the characteristics summarized in Table 1 with illustrating examples in Fig. 3. F1 represents clay-rich hemipelagite and F2 represents clay-poor volcaniclastic deposits. Facies F2 is further subdivided into carbonate-rich F2a and carbonate-poor F2b facies. Assigning the volcaniclastic beds to fallout, primary and secondary turbidite classes was then a complex task involving an assessment of all the data available, bearing in mind the considerations above. In the following results, we highlight observations that support these choices of classes. Those interpretations are shown in the interpretation columns of Fig. 2. The full characteristics and interpretations of individual volcaniclastic-rich layers are provided in Supplementary Data Electronic Appendix 1.

Facies visual descriptions

The sediment was first classified into two facies (F1 and F2) based on the relative abundance of clay and volcaniclastic particles. F1 is mainly composed of homogenous ungraded pale brown/grey mud to silt. Mottled structures, dispersed tephra grains and gradual colour changes are common (Fig. 3a). The abundance of microfossils in F1 is intermediate to high.

F2 includes clay-poor volcaniclastic-rich deposits. The grain sizes of F2 beds vary from fine (silt to fine sand) to coarse (medium sand to pebble) beds. F2 varies in colour from light to dark brown (Figs. 3b–3g). Basal bed contacts are commonly sharp but upper bed contacts can be gradual and diffuse. Sedimentary structures typical of turbidites are common, such as laminations, ripples, internal erosive surfaces and normally graded sequences (cf. Bouma 1962; Stow and Piper 1984; Talling *et al.* 2012), though inverse grading occasionally appears in the middle of beds (Fig. 3d). Turbidite structures are

328 more apparent in coarse-grained than in fine-grained deposits (Figs. 3c to 3e). Burrows
329 (bioturbation) are more common in fine-grained deposits (Figs. 3c, 3e, 3f and 3g).

330 ***Interpretation***

331 F1 was formed of fine grains and microfossils such as foraminifers deposited by settling
332 in a largely quiescent ambient environment. Mottled structures are caused by mud-
333 feeding biota burrowing the sediment which are commonly observed in (hemi)pelagic
334 beds (Wetzel and Uchman 2012). Dispersed volcanic shards are the results from either
335 bioturbation or later settling of ash transported by varied processes through water
336 column (Scudder *et al.* 2016). The gradual and slight colour variations of these beds are
337 associated with varied organic matter content and redox variations (e.g., Savrda *et al.*
338 2001; Hoogakker *et al.* 2004). Bioturbation can incorporate particles from nearby beds,
339 which may explain dark patches of volcanic-rich sediment found in the two analysed
340 hemipelagic samples (e.g., core 1226 at 55 and 167 cm).

341 The volcaniclastic particles in F2 could be derived either directly from volcanic activity
342 (e.g., pyroclastic fallout or primary volcaniclastic density currents) or from reworking
343 of volcanic material (e.g., submarine landsliding and coastal erosion). In many cases,
344 the fallout beds contain normally-graded vesicular pyroclastic particles with a higher
345 concentration of crystals at their bases and are commonly bioturbated at their tops
346 (Carey and Schneider 2011). Although normal-grading and bioturbation structures can
347 also commonly appear in the primary and secondary volcaniclastic turbidites,
348 coexisting laminated sedimentary structures and ripples more likely originated from
349 sediment density currents (Bouma 1962; Stow and Piper 1984; Talling *et al.* 2012). We
350 interpret crudely-graded/structureless coarse-grained beds with erosive basal contacts
351 as corresponding with sandy Bouma sub-divisions T_a, laminated coarse-grained beds
352 as corresponding with sandy Bouma sub-divisions T_b to T_c, and fine-grained beds with

poorly developed lamination with T_d to T_e (Bouma 1962; Walker 1978). Material such as shelf-origin coralline algae debris and shell fragments (Figs. 5e and 5f) admixed in these volcaniclastic deposits also favor emplacement by turbidity currents over a pyroclastic fallout origin. However, we are also aware that the typical characteristics of fallout deposits and turbidites may be obscured or modified by post-depositional bioturbation. The complexity and part similarity of sedimentary structures between different types of volcaniclastic deposits reflect that other parameters are still needed to assure the emplacement mechanism interpretation.

Volcanic glass geochemistry

Examples of geochemical variations in MgO and SiO_2 of volcanic glasses extracted from F2 beds are shown in Figs. 4 and 11 (full glass data are provided in Supplementary Data Electronic Appendix 2). Major element concentrations of volcanic glasses can be classified as three groups based on composition. The geochemical compositions of the volcaniclastic beds in two of the groups tend to cluster tightly (e.g., core 1230 at 158–160 cm shown in Fig.4), though rare outliers occur more often in one of them (e.g., core 1230 at 138–140 cm shown in Fig. 4). The last group, in contrast, have a scattered range of geochemical compositions (e.g., core 1215 at 208–210 cm shown in Fig. 4).

Interpretation

A relatively homogeneous chemical composition of vitric particles in a volcaniclastic-rich bed favours a primary syn-eruptive origin, suggesting a probable origin by either fallout or discharge of pyroclastic flows into the sea where they transformed into turbidity currents without significantly eroding earlier volcaniclastic substrates of other compositions (Carey and Schneider 2011). Volcanic glasses transported through primary processes usually cluster in a narrow range of geochemical compositions due

to little mixing with older tephras, although eruptions of compositionally zoned magma or old strata exhumed can produce a genetically related range of glass compositions in the deposit. While the structural and textural appearance of secondary turbidites formed by reworking of volcaniclastic materials is very similar to that of primary turbidites, the glass particles commonly display a broad compositional spectrum instead of a tight cluster because of mixing of particles from multiple sources. Such mixtures can originate from a wide choice of processes ranging from exposed tephra particles eroded by wind and water (Carey and Sigurdsson 1984; Reid *et al.* 1996; Le Friant *et al.* 2004) to large-scale mass wasting such as submarine landsliding (Moore *et al.* 1994; Masson *et al.* 2006). However, whether chemical variation is compositionally homogeneous or heterogeneous may be not so straightforward sometimes, so other information is required to reduce uncertainty of interpretation.

Morphologies of volcanic grains

Three examples were selected to illustrate the morphometric features of the different types of volcaniclastic deposits along with their geochemical compositions (Fig. 4; full set of morphometric measurements in Supplementary Data Electronic Appendix 3). There is no or only a slight systematic variation of either NPL or aspect ratio with grain size for individual samples (Fig.4). We chose a limiting NPL value of 1.28 to sub-divide the samples into two groups as shown in Fig. 6a (black and red colours). There is apparently no corresponding difference in aspect ratio between the two groups (Fig. 6b).

Interpretations

The shapes of volcanic particles can be clues of transport process (e.g., Manga *et al.* 2011; Cassidy *et al.* 2014). Abrasion and comminution of clasts both can occur during

401 transport (e.g., Walker 1981). Abrasion is expected to increase the roundness of clasts,
402 whereas comminution may decrease roundness. Angular and elongated particles are
403 interpreted to have experienced less grain-grain interactions than rounded and
404 equidimensional particles (e.g., Manga *et al.* 2011; Cassidy *et al.* 2014). Angular
405 particles are typical for air-transmitted deposits from low-concentration ash clouds with
406 few grain-grain contacts while rounded particles are commonly observed in deposits
407 from sediment flows, particularly those in which high particle concentration or intense
408 bed-load transport produce frequent intense particle contacts (Wilson and Hildreth
409 1998). Cassidy *et al.* (2014) also suggested that particles emplaced purely by air should
410 be distinguishable from particles emplaced in sedimentary flows if the later involve
411 intense grain-grain interactions that cause grains to progressively become more
412 spherical and develope smooth surfaces.

413 As expected, the suggested pyroclastic fallout deposits have NPL values that are higher
414 on average and more varied than those of the suggested secondary turbidite deposits
415 (Fig. 4). However, the NPL values of the primary turbidite deposits can be either high
416 or low. Considering that the cores are in proximal locations, the varied NPL values of
417 the primary turbidite deposits may be due to the short distance of transportation,
418 reducing the time for abrasion. Although the NPL values of fallout deposits are distinct
419 from secondary turbidite deposits, a combination of chemical compositions and
420 sedimentary structures are still required to convincingly separate fallout deposits from
421 primary turbidite deposits.

422 Particles with high NPL are angular and/or elongated; hence aspect ratio is also
423 potentially useful to assess the contribution of elongation to NPL values. The samples
424 of the high NPL group do not typically have high aspect ratios, so the high NPL values
425 are mainly due to grain angularity rather than elongation, as can be seen in sample

426 photos (Figs. 5a, b). While angularity (NPL) is reduced by abrasion (Krumbein 1941),
427 elongation (aspect ratio) will mainly be reduced by comminution. The similarity of
428 aspect ratios between the high and low NPL groups in Fig. 6 implies that particles have
429 only become moderately rounded by abrasion and have not broken up greatly during
430 transport. Alternatively, the source eruptions did not produce significant amounts of
431 elongated grains.

432 ***Bulk mineral assemblage***

433 The XRD data of the F2 volcaniclastic turbidites (Fig. 7) revealed volcanic minerals
434 (anorthoclase, plagioclase, clinopyroxene, olivine, amphibole and biotite, which are
435 phenocryst phases found in the mildly alkalic or peralkaline volcanic rocks on the
436 Azores islands), marine authigenic and biogenic minerals (e.g., calcite and aragonite)
437 and quartz. Comparatively high abundances of amorphous material exist in some
438 samples and was microscopically identified as glass shards.

439 The light-coloured F2 volcaniclastic turbidites possess more biogenic material (up to
440 25%) than the dark-coloured F2 turbidites (~5%), although mineralogical assemblages
441 are otherwise similar. We sub-divided facies F2 into F2a and F2b based on carbonate
442 contents of >10% and <10%, respectively (Fig. 7). The biogenic material was
443 microscopically identified as foraminifera, shell fragment and coralline algae debris
444 (e.g., Figs. 5e and 5f). High carbonate percentages can exist in both primary (e.g., 1230-
445 332) and secondary turbidites (e.g., 1215-214).

446 ***Interpretation***

447 The bulk mineral assemblages of the samples are similar to those on the present-day
448 shelf (e.g., Valente 2020), although carbonate contents on the shelf vary more greatly
449 and are generally higher (10–90%; Quartau et al., 2015) compared to our F2a

450 volcaniclastic beds (<25%; Fig.7). Remobilization of shelf biogenic material or slope
451 particles originating from shelf spill-over should be the cause of higher carbonate
452 concentrations in F2a than F2b volcaniclastic turbidite deposits, given that most of the
453 biogenic material occurring in F2a is of shelf origin (Figs. 5e and 5f; Wisshak et al.,
454 2014). The low carbonate content in F2b could be attributed to the lack of incorporated
455 of shelf origin bioclasts. For example, volcaniclastic grains may have only settled
456 through the water column (e.g., pyroclasic fallout) or transported over a carbonate-
457 starved shelf platform. Remobilization can occur in either primary or secondary
458 turbidity currents. For instance, primary volcaniclastic density flows can incorporate
459 unconsolidated shelf bioclasts (e.g., Whitham 1989; Trofimovs *et al.* 2008).
460 Alternatively, volcanic island submarine slopes or outer shelves may become unstable
461 and collapse, sourcing secondary turbidity currents containing both volcaniclastics and
462 bioclasts (e.g., Quartau *et al.* 2015). The high fraction of glass in the volcaniclastic-rich
463 deposits can also indicate the origin of the primary volcaniclastic material. Scarcity of
464 volcanic glass or mixture of volcanic glass compositions probably imply re-deposition
465 from terrestrial deposits.

466 ***Total organic carbon, total nitrogen, and carbon isotopes***

467 All facies have low organic carbon contents (Fig. 8; full data are provided in
468 Supplementary Data Electronic Appendix 4). F1 has the highest (>0.15 wt%), F2a has
469 intermediate (slightly > 0.1 wt%) and F2b has the lowest organic carbon content (<0.1
470 wt%). Fine-grained samples of F2a (light orange bars in Fig.8) have slightly higher
471 organic matter contents on average than the coarse-grained samples of F2a (dark orange
472 bars in Fig.8). The F2a TOC/TN ratios are 5–15 and $\delta^{13}C$ values are -18‰ to -25‰
473 (Fig. 9). The corresponding values for the F2b samples are 5–10 and -22‰ to -27‰,
474 respectively.

475 ***Interpretation***

476 The overall low TOC contents could be attributed to low input of organic matter and
477 poor preservation after deposition, such as slow sediment accumulation rates and
478 oxidised bottom water bodies (Cowie *et al.* 1995). Although lying around the analytical
479 detection limit, the lower TOC contents of F2b compared with F2a are consistent with
480 less or no mobilised shelf or submarine slope biogenic material in F2b, supporting a
481 primary volcaniclastic interpretation for F2b in this study.

482 The TOC/TN ratios and $\delta^{13}C$ values help to constrain the origins of the organic matter.
483 According to Meyers (1994), TOC/TN ratios of algae typically vary from 4 to 10,
484 whereas ratios for land plants are usually >20. Marine organic matter typically has
485 average $\delta^{13}C$ values between -22 and -20‰. C_3 and C_4 land plants have average $\delta^{13}C$
486 values of -27‰ and ~ -14‰, respectively. The TOC/TN ratios and $\delta^{13}C$ values of our
487 samples show a dominant marine-algal origin. The F1 and F2a samples also contain
488 minor carbon from land plants (Fig. 9). The organic matter in some F2b samples
489 appears to originate from freshwater algae, likely derived from island drainage.

490 The modestly higher organic matter concentration in F2a than in F2b (Fig.8) suggests
491 incorporation by turbidity currents of shelf or slope material (e.g., Figs 5e and 5f)
492 containing some organic matter and its subsequent preservation by rapid burial.
493 Although shallow sediments lie in an oxidising environment, organic matter
494 preservation is also facilitated by the high productivity of coastal seas (Martin *et al.*
495 1987) and the effects of bioturbation (Emerson and Hedges 1988). The higher organic
496 matter concentration in finer-grained sediments (F2a) than those in coarse-grained
497 sediments (F2b) may be an effect of total particle surface area (Bergamaschi *et al.*

498 1997). Organic matter can be absorbed on mineral surfaces, protecting it and slowing
499 the rate of remineralisation (Keil *et al.* 1994).

Discussion

In total 42 volcaniclastic-rich beds were identified. Among these volcaniclastic beds, 24 of them are F2a and 18 of them are F2b. F2a comprises 4 pyroclastic fallout beds, 8 primary turbidites and 13 secondary turbidites. F2b comprises 5 pyroclastic fallout beds and 11 primary turbidites. Although the lack of biogenic material was a characteristic used to discriminate primary and secondary volcaniclastic deposits in offshore Montserrat (Trofimovs et al., 2013; Le Friant et al., 2015), 12 primary volcaniclastic beds have relatively high carbonate contents in these cores. This could be attributed to the incorporation of shelf sediments during transport and/or intense post-depositional bioturbation mixing carbonate particles from the tops or bases of beds (e.g., core 1226 at 18–40 cm). Therefore, we highlight that other data are still needed to interpret transportation mechanisms instead of counting individual characteristics, as illustrated here.

Assigning uncertainties to the volcaniclastic bed emplacement interpretations (fallout, and primary and secondary volcaniclastic turbidites) is difficult given the many parameters were used. Those emplacement interpretations are less certain where individual parameters do not indicate bed type clearly (e.g., core 1215 at 133–137 cm and core 1230 at 78–86 cm). Nevertheless, in most samples, all parameters indicated the emplacement type consistently, so the above relative proportions of different types should be reliable. To allow readers to assess the interpretations for themselves, the full set of sample classifications and parameters is included in Appendix 1.

Landslide scars such as those in Fig. 1b are common around the Azores islands and earthquakes potentially triggering slope failure are frequent, suggesting that associated turbidity currents should occur frequently. The modal volume of landslide scars for Faial, Pico, São Jorge and Terceira lies in the 10^5–10^6 m^3 range (Chang *et al.* in review).

525 If a 10^6 m^3 volume of mobilised slope sediment were distributed uniformly over basins
526 of roughly 20*20 km dimensions (Fig. 1a), they would generate deposits of 2.5 cm in
527 thickness. Although having only half the 10^5–10^6 m^3 frequency, scars an order of
528 magnitude larger in volume are also common, Therefore, secondary volcaniclastic
529 deposits of 2.5–25 cm thickness derived from slope failure should be common.

530 The results summarised in Fig. 2 (right-most column), however, suggests that
531 secondary volcaniclastic deposits are not the overwhelming majority. Rather the cores
532 are dominated by primary volcaniclastic turbidites, particularly in cores 1226 and 1230.
533 We interpret the dominance of primary over secondary turbidites as either due to
534 sedimentary flows generated by slope failure not all running out to the basin floors or
535 to volcanic eruptions generating the primary beds being more frequent than the slope
536 failures or some combination of these effects.

537 *Origins of volcaniclastic turbidites*

538 Primary volcaniclastic turbidites should mostly reflect adjacent eruption history rather
539 than more distant eruptions. Hence, those in core 1219 should be mainly sourced from
540 Caldera Volcano on Faial island (Fig. 1), although the Capelo Volcanic Complex is
541 another possibility. The site is also flanked by submarine cones of NW São Jorge and
542 NW Faial, although it is currently unclear how active they are (Mitchell *et al.* 2018).
543 Those in core 1230 could be sourced from Santa Bárbara or Pico Alto volcanoes on
544 Terceira. The primary volcaniclastic turbidites in core 1215 may originate from Pico
545 and/or São Jorge Islands. Core 1226 within the Terceira Rift may have received primary
546 volcaniclastic turbidites from Terceira or from submarine eruptions on the Serreta
547 Ridge, which is volcanically active (Gaspar *et al.* 2003). The upper submarine slopes
548 of the islands contain abundant scars from upper-slope landslides and retrogressive

549 failures in their outer shelves (Fig. 1B), so they are potential sources of the secondary
550 volcaniclastic turbidites. Emplacements of secondary volcaniclastic turbidites seem to
551 be randomly distributed in each core and there are no clear major differences in
552 occurrences between them. Their common occurrences amongst the cores could
553 ultimately reflect triggering of slope failure around all the islands, such as by
554 earthquakes or storm waves.

555 *Applicability of morphologic analysis of volcanic grains in other volcanic settings*

556 Cassidy et al. (2014) presented volcanic grain morphometric data for volcaniclastic
557 beds that had known transport origins. Our analysis method differs from theirs as we
558 measured fewer grains in each sample and classified deposits using a different
559 parameter, normalised perimeter distance (NPL), so we have investigated if our method
560 would also separate the samples of Cassidy et al. (2014) into the same two groups
561 assigned by them.

562 The results shown in Fig. 10 have both slightly lower average and standard deviation
563 of NPL and aspect ratio than those of the Azorean samples in Fig. 6. The 1.23–1.20
564 NPL value that allows a separation between two types of deposits in the results of
565 Cassidy et al. (2014) is smaller than 1.28 in Fig. 6. This difference might be either due
566 to higher angularity of grains in the Azores cores or to the ~300 volcanic grains
567 measured by Cassidy et al. (2014) compared with only 30–60 in each of our samples.
568 If the number of grains measured were important, we would expect a more confined
569 range and perhaps also a lower separation value of NPL in the Azorean samples if more
570 measurements were made. Otherwise, a unique separation value of NPL may be found
571 in each volcanic setting if the morphometric characteristics are dominantly controlled
572 by original characteristics such as solid and bulk densities, vesicle textures, primary

573 particle shapes and glass/crystal ratios. Although slight differences exist in the two sets
574 of results, both sets of graphs still show pyroclastic fallout tending to have a higher
575 average and variability of NPL than the deposits emplaced by turbidity currents. This
576 consistency suggests that the more limited morphometric analysis conducted here is
577 effective and potentially could be applied to other volcanic settings.

578 *Lateral correlation of pyroclastic fallout beds*

579 The glass shard compositions cluster tightly in each of the four cores but differ between
580 the cores, apart from a few outliers (Fig. 11). This suggests that fallout beds cannot be
581 correlated between cores and that each core had its own volcanic source. The highly
582 evolved glasses in core 1230 taken north of Terceira derive from the
583 trachytic/comenditic eruptions on that island (cf. Calvert et al. 2006; Jeffery et al.,
584 2018). Ashes with such evolved compositions did not reach core 1226 between
585 Terceira, Graciosa and São Jorge, which only contains mafic glass shards. The
586 compositions of core 1226 differ from those of glass shards in cores 1215 and 1219
587 between Faial, Pico and São Jorge, suggesting a closer source, such as basaltic eruption
588 on Terceira (Self et al. 1976) or at the Serreta Ridge. Association of the glass shards in
589 cores 1215 and 1219 with sources on the surrounding islands is not presently possible,
590 although dating and trace element glass analyses in the future may help. Although
591 sedimentation rates vary with bathymetry and distance from islands, the most extensive
592 volcanic history preserved in those cores is <100 ky, which is roughly estimated from
593 the length of hemipelagic sediments (F1) divided by the hemipelagic sedimentation rate
594 (3.5 cm/ky) in the central Azores basin (Vlag *et al.* 2004). Hence, the cores contain a
595 comparable range of eruption history to deposits on the islands and partly within ^{14}C
596 dating range.

Comparing thicknesses of volcaniclastic beds with those near other oceanic islands

Thickness frequency distributions have been used to characterise turbidite sequences from other settings (Hiscott *et al.* 1992; Beattie and Dade 1996; Talling 2001). Such thickness frequency distributions can reflect the relative importance of large versus small turbidite beds. For example, volcaniclastic beds in the Izu-Bonin forearc basin show such a distribution with a magnitude of the gradient β slightly above 1.0 (purple dashed line in Fig. 12c; Hiscott *et al.,* 1992).

We use the similar approach, which is useful to compare volcaniclastic bed abundances over certain thickness ranges between the islands. A limited dataset of volcaniclastic bed thicknesses was obtained from near Gran Canaria (Sumita and Schmincke, 1998), Reunion (Saint-Ange *et al.* 2013), the Cape Verde islands (Eisele *et al.* 2015a, b) and the Azores, which allows comparison between island groups of contrasting volcanic history and core sampling proximity to the islands. Due to the varied and commonly less detailed analyses that are available for these cores compared with the Azores cores, the different types of volcaniclastic beds were typically not all well discriminated and some may have been overlooked where they had weakly contrasting colour with other sediments. To compare with the Azores results on the same basis, therefore, we counted bed thicknesses from all types of volcaniclastic-rich beds in each site as though they were a single type.

The results in Fig. 12 show that the central Azores and Cape Verde islands have similar thickness distributions, with both commonly having 2–20 cm volcaniclastic beds. Although the length of cores from the central Azores and Cape Verde islands are too limited to determine their complete distributions, the graphs are compatible with rapid declines in frequency after the peaks, suggesting that small beds are important over the sediment depth sampled by coring.

622 The Gran Canaria cores (Fig. 12c), in contrast, have more than an order of magnitude
623 smaller frequency of decimetre-scale beds than either the Azores or Cape Verdes cores.
624 The shallow graph gradient (small magnitude of β) for the data above $\log_{10}(T)$ of 0.5
625 shows that the larger beds are proportionally more important relative to small beds than
626 for the Izu-Bonin cores (purple dashed line in Fig. 12c; Hiscott et al., 1992). Core logs
627 of Gran Canaria shown in Schmincke and Sumita (1998; their figure 21) are also
628 noticeably episodic, with typically 20 m non-volcaniclastic-rich intervals between
629 clusters of volcaniclastic beds. Both features reflect a different volcanic evolution of
630 Gran Canaria, which was episodic and explosive over the period of volcano emergence
631 from the sea that the cores span.

632 The Reunion island cores were collected on the dipping volcaniclastic apron of the
633 island, at varied distances from the shoreline (Saint-Ange *et al.* 2013), offshore an
634 embayment of the island containing collapse structures (e.g., Ollier *et al.* 1998). Fig.
635 12d shows a high frequency of volcaniclastic beds and a high average bed thickness
636 (>20 cm). The cores commonly contain coarse and poorly-sorted turbidites, so their
637 formative turbiditity currents may have been in the upper flow regime or at least more
638 vigorous than the Azores turbidity currents. The cores were also collected on a slope
639 close to a large slump scar, so slope movements may have originated the turbidity
640 currents.

Conclusions

The four selected Azorean sediment cores contain three sedimentary facies recognised on the basis of sedimentary logging (visual and microscope inspection), geochemical compositions (bulk mineralogy assemblage from XRD measurements, electron microprobe analysis of volcanic glass shards, carbon isotopy and total organic carbon and nitrogen) and morphometric analysis of volcanic grain shapes (angularity and elongation). They are: F1, clay-rich hemipelagite, F2a, clay-poor and carbonate-rich volcaniclastic deposits, and F2b, clay-poor and carbonate-poor volcaniclastic deposits. Mottled structures caused by bioturbation are common in F1 and sometimes in fine-grained F2. Normally graded, laminated beds with sharp bases are commonly identified in F2a and F2b. All three facies typically possess high contents of volcanogenic minerals and comparatively low organic carbon. F2a possess more carbonate (10–20%) and organic carbon (>0.1 wt%) than F2b, likely from carbonate material incorporated from the shelf and/or submarine slope.

The processes by which the F2 volcaniclastic deposits were emplaced, whether primary or secondary, was determined based on multiple lines of evidence. Primary and secondary volcaniclastic turbidites contain structures associated with turbidity currents and can also contain high amounts of shelf-derived carbonate. Secondary turbidites contain rounded volcaniclastic grains, and their volcanic glass shards have heterogeneous chemical compositions. Primary volcaniclastic grains, in contrast, can be either angular or rounded. Their volcanic glass compositions tend to cluster in a narrow range, sometimes with rare outliers, although a range of glass compositions genetically related to magma fractionation can also be observed. Although the sedimentary structures and chemical compositions of fallout deposits can be similar to primary volcaniclastic turbidites, angular particles and scarcity of biogenic carbonate

favour a fallout interpretation. However, depositional environments with intense post-depositional bioturbation can obscure all these suggested characteristics.

Interpreting individual event beds and the mechanisms that emplaced them remains a challenge, although the approach of using multiple characteristics presents a way forward here. Provisional analysis of volcanic glass compositions has revealed that individual cores tend to have relatively homogeneous compositions, which would not be expected if they originated from different islands or source volcanoes. Hence, volcaniclastic beds in the Azorean cores reflect the eruption histories of adjacent islands rather than regional events.

Bed thickness-frequency distributions were used to contrast the volcaniclastic emplacement histories of four island groups. Those distributions for the central Azores and Cape Verde islands are similar, possibly reflecting their similar bed origins. The decimetre beds for Gran Canaria cores are at least an order of magnitude less abundant than the central Azores. That small gradient (β) reflects the large-volume explosive eruptions that occurred during the volcano emergence stage of Gran Canaria, which led to many dominating larger volcaniclastic beds. The cores of Reunion contain poorly sorted, coarser and thicker beds on average than those of the Azores, partly reflecting emplacement by larger and more vigorous turbidity currents.

Acknowledgements

YCC thanks the editors Sebastian Watt and reviewers James Hunt and Ricardo Ramalho and for providing their constructive comments, which led to significant improvements of this manuscript. the government of Taiwan for funding this research with a PhD scholarship. We thank the scientific party and crew of RV *Meteor* during cruise M141/1 for their work in collecting the gravity cores, Steffen Kutterolf and Line Herberg provided data for part of the EMP samples, Doris Maicher for help to shift heavy cores from the GEOMAR repository, Bart Van Dongen for use of laboratory space for sample preparation, Elsa-Marie Portanyi for working together on setting up the preliminary chemical experiments, Kévin Boulesteix for sharing his knowledge of ichnology, Emíly D. Flud, Shunwen Yu, Yu-Huang Chen, Hsing-Chien Juan and Chia-Yu Lin for discussions on the geochemical analyses, John Waters for the XRD measurements and analysis, Alastair Bewsher for the pre-testing the TOC analyses in Manchester (data not shown), Stephen Crowley for the TOC, TN and $\delta^{13}C$ analyses in the University of Liverpool, Michael Cassidy advice on morphometric analysis and Rui Quartau for providing high-resolution multibeam data from around Terceira displayed in Fig. 1. The latter data were acquired during project "Features of Azores and Italian Volcanic Islands (FAIVI)", supported by the European Communities 7th Framework Programme under EUROFLEETS grant agreement no. 228344. Travel to Germany was funded by an International Exchanges grant from the Royal Society (IES\R3\170081).

References

Ávila, S.P., Cordeiro, R., Rodrigues, A.R., Rebelo, A.C., Melo, C., Madeira, P. and Pyenson, N.D. 2015. Fossil Mysticeti from the Pleistocene of Santa Maria Island, Azores (Northeast Atlantic Ocean), and the prevalence of fossil cetaceans on oceanic islands. *Palaeontol. Electron*, **18**, 1-12, https://doi.org/10.26879/548.

Beattie, P.D. and Dade, W.B. 1996. Is scaling in turbidite deposition consistent with forcing by earthquakes? *J. Sed. Res.*, **66**, 909-915, https://doi.org/10.1306/D4268437-2B26-11D7-8648000102C1865D.

Bergamaschi, B.A., Tsamakis, E., Keil, R.G., Eglinton, T.I., Montluçon, D.B. and Hedges, J.I. 1997. The effect of grain size and surface area on organic matter, lignin and carbohydrate concentration, and molecular compositions in Peru Margin sediments. *Geochimica et Cosmochimica Acta*, **61**, 1247-1260, https://doi.org/10.1016/S0016-7037(96)00394-8.

Bonadonna, C., Mayberry, G. *et al.* 2002. Tephra fallout in the eruption of Soufrière Hills Volcano, Montserrat. *Geological Society, London, Memoirs*, **21**, 483-516, https://doi.org/10.1144/GSL.MEM.2002.021.01.22.

Bonatti, E. 1990. Not so hot "hot spots" in the oceanic mantle. *Science*, **250**, 107-111, https://doi.org/10.1126/science.250.4977.107.

Bouma, A.H. 1962. *Sedimentology of some Flysch deposits; A graphic approach to facies interpretation*. Elsevier Pub. Co., Amsterdam; New York.

Boygle, J. 1999. Variability of tephra in lake and catchment sediments, Svínavatn, Iceland. *Global and Planetary Change*, **21**, 129-149, https://doi.org/10.1016/S0921-8181(99)00011-9.

Calder, E.S., Cole, P.D. *et al.* 1999. Mobility of pyroclastic flows and surges at the Soufriere Hills Volcano, Montserrat. *Goephys. Res. Lett.*, **26**, 537-540, https://doi.org/10.1029/1999GL900051.

Calvert, A.T., Moore, R.B., McGeehin, J.P. and Rodrigues da Silva, A.M. 2006. Volcanic history and $^{40}Ar/^{39}Ar$ and ^{14}C geochronology of Terceira Island, Azores, Portugal. *J. Volcanol. Geother. Res.*, **156**, 103-115, https://doi.org/10.1016/j.jvolgeores.2006.03.016.

Cappello, A., Geshi, N., Neri, M. and Del Negro, C. 2015. Lava flow hazards—An impending threat at Miyakejima volcano, Japan. *J. Volcanol. Geother. Res.*, **308**, 1-9, https://doi.org/10.1016/j.jvolgeores.2015.10.005.

Carey, S. and Sigurdsson, H. 1984. A model of volcanogenic sedimentation in marginal basins. *Geological Society, London, Special Publications*, **16**, 37-58, https://doi.org/10.1144/gsl.Sp.1984.016.01.04.

Carey, S., Maria, T. and Cornell, W. 1998. Processes of volcaniclastic sedimentation during the early growth stages of Gran Canaria based on sediments from Site 953. *In*: Weaver, P.P.E., Schmincke, H.-U., Firth, J.V. and Duffield, W. (eds) *Proc. Ocean Drill. Progr., Sci. Res. Vol. 157*. Ocean Drilling Program, College Station, Texas, 183-200, https://doi.org/doi:10.2973/odp.proc.sr.157.119.1998.

Carey, S.N. and Schneider, J.-L. 2011. Chapter 7 - Volcaniclastic Processes and Deposits in the Deep-Sea. *In*: HüNeke, H. and Mulder, T. (eds) *Developments in Sedimentology*. Elsevier, 457-515, https://doi.org/10.1016/B978-0-444-53000-4.00007-X.

Casalbore, D., Clare, M.A. *et al.* 2020. Bedforms on the submarine flanks of insular volcanoes: New insights gained from high resolution seafloor surveys. *Sedimentology*, https://doi.org/10.1111/sed.12725.

Cassidy, M., Watt, S.F.L., Palmer, M.R., Trofimovs, J., Symons, W., Maclachlan, S.E. and Stinton, A.J. 2014. Construction of volcanic records from marine sediment cores: A review and case study (Montserrat, West Indies). *Earth-Sci. Rev.*, **138**, 137-155, https://doi.org/10.1016/j.earscirev.2014.08.008.

Chang, Y.-C., Mitchell, N., Quartau, R. and Hansteen, T. 2019. Size Distribution and Causes of Submarine Landslides, Central Azores Islands. *Geophysical Research Abstract, EGU General Assembly*, Vienna, Austria.

Chang, Y.-C., Mitchell, N., Quartau, R. and Hansteen, T. in review. Landslides in the Upper Submarine Slopes of Volcanic Islands: the Central Azores. *Geochemistry, Geophysics, Geosystems*.

Charlier, B.L.A., Ginibre, C., Morgan, D., Nowell, G.M., Pearson, D.G., Davidson, J.P. and Ottley, C.J. 2006. Methods for the microsampling and high-precision analysis of strontium and rubidium isotopes at single crystal scale for petrological and geochronological applications. *Chem. Geol.*, **232**, 114-133, https://doi.org/10.1016/j.chemgeo.2006.02.015.

Christopher, T.E., Humphreys, M.C.S., Barclay, J., Genareau, K., De Angelis, S.M.H., Plail, M. and Donovan, A. 2014. Chapter 17 Petrological and geochemical variation during the Soufrière Hills eruption, 1995 to 2010. *Geological Society, London, Memoirs*, **39**, 317-342, https://doi.org/10.1144/m39.17.

Cole, P., Guest, J., Duncan, A. and Pacheco, J.-M. 2001. Capelinhos 1957–1958, Faial, Azores: deposits formed by an emergent surtseyan eruption. *Bulletin of Volcanology*, **63**, 204-220, https://doi.org/10.1007/s004450100136.

Cowie, G., Hedges, J., Prahl, F. and De Lange, G. 1995. Elemental and major biochemical changes across an oxidation front in a relict turbidite: an oxygen effect. *Geochimica et Cosmochimica Acta*, **59**, 33-46, https://doi.org/10.1016/0016-7037(94)00329-K.

Cronin, S.J., Neall, V.E., Lecointre, J.A. and Palmer, A.S. 1997. Changes in Whangaehu river lahar characteristics during the 1995 eruption sequence, Ruapehu volcano, New Zealand. *J. Volcanol. Geother. Res.*, **76**, 47-61, https://doi.org/10.1016/S0377-0273(96)00064-9.

Dengler, A.T., Wilde, P., Noda, E.K. and Normark, W.R. 1984. Turbidity currents generated by Hurricane Iwa. *Geo-Mar. Lett.*, **4**, 5-11, https://doi.org/10.1007/BF02237967.

Eisele, S., Freundt, A., Kutterolf, S., Ramalho, R.S., Kwasnitschka, T., Wang, K.L. and Hemming, S.R. 2015a. Stratigraphy of the Pleistocene, phonolitic Cão Grande Formation on Santo Antão, Cape Verde. *J. Volcanol. Geother. Res.*, **301**, 204-220, https://doi.org/10.1016/j.jvolgeores.2015.03.012.

Eisele, S., Reißig, S., Freundt, A., Kutterolf, S., Nürnberg, D., Wang, K.L. and Kwasnitschka, T. 2015b. Pleistocene to Holocene offshore tephrostratigraphy of highly explosive eruptions from the southwestern Cape Verde Archipelago. *Marine Geology*, **369**, 233-250, https://doi.org/10.1016/j.margeo.2015.09.006.

Emerson, S. and Hedges, J. 1988. Processes controlling the organic carbon content of open ocean sediments. *Paleoceanography*, **3**, 621-634, https://doi.org/10.1029/PA003i005p00621.

Féraud, G., Kaneoka, I. and Allegre, C.J. 1980. K/Ar ages and stress pattern in the Azores: dynamic implications. *Earth Planet. Sci. Lett.*, **46**, 275-286, https://doi.org/10.1016/0012-821X(80)90013-8.

Fisher, R.V. 1961. Proposed classification of volcaniclastic sediments and rocks. *Geol. Soc. Am. Bull,*, **72**, 1409-1414, https://doi.org/10.1130/0016-7606(1961)72[1409:PCOVSA]2.0.CO;2.

Forjaz, V. 1968. Carta geológica do sistema vulcânico Faial-Pico-S. Jorge. Escala 1: 200 000. *A actividade vulcânica na ilha do Faial (1957 67)*.

Fornari, D.J., Malahoff, A. and Heezen, B.C. 1979. Submarine slope micromorphology and volcanic substructure of the island of Hawaii inferred from visual observations made during U.S. Navy deep-submergence vehicle (DSV) "Sea Cliff". *Marine Geology*, **32**, 1-20, https://doi.org/10.1016/0025-3227(79)90143-9.

Freundt, A. and Schmincke, H.-U. 1995. Petrogenesis of rhyolite-trachyte-basalt composite ignimbrite P1, Gran Canada, Canary Islands. *Journal of Geophysical Research: Solid Earth*, **100**, 455-474, https://doi.org/10.1029/94JB02478.

Gaspar, J.L., Queiroz, G., Ferreira, T., Medeiros, A.R., Goulart, C. and Medeiros, J. 2015. Chapter 4 Earthquakes and volcanic eruptions in the Azores region: geodynamic implications from major historical events and instrumental seismicity. *Geological Society, London, Memoirs*, **44**, 33-49, https://doi.org/10.1144/m44.4.

Gaspar, J.L., Queiroz, G., Pacheco, J.A., Ferreira, T., Wallenstein, N., Almeida, M.H. and Coutinho, R. 2003. Basaltic lava balloons produced during the 1998-2001 Serreta Submarine Ridge eruption (Azores). *In*: White, J.D.L., Smellie, J.L. and Clague, D.A. (eds) *Subaqueous Explosive Volcanism, Am. Geophys. Union Geophysical Monogr. 140*. Am. Geophys. Union, Washington, DC, 205-212, https://doi.org/10.1029/140GM13.

Gente, P., Dyment, J., Maia, M. and Goslin, J. 2003. Interaction between the Mid-Atlantic Ridge and the Azores hot spot during the last 85 Myr: Emplacement and rifting of the hot spot-derived plateaus. Geochem. Geophys. Geosys., 4, https://doi.org/8510.1029/2003GC000527.

Gertisser, R., Self, S. *et al.* 2010. Ignimbrite stratigraphy and chronology on Terceira Island, Azores. *The Geological Society of America, Special Paper*, **464**, 133-154, https://doi.org/10.1130/2010.2464(07).

Gudmundsdóttir, E.R., Eiríksson, J. and Larsen, G. 2011. Identification and definition of primary and reworked tephra in Late Glacial and Holocene marine shelf sediments off North Iceland. *Journal of Quaternary Science*, **26**, 589-602, https://doi.org/10.1002/jqs.1474.

Hansteen, T.H., Freundt, A. and Kutterolf, S. 2017. *Short cruise report RV METEOR M141/1: Azores tephras.* GEOMAR Helmholtz-Zentrum für Ozeanforschung Kiel.

Hildenbrand, A., Madureira, P., Marques, F.O., Cruz, I., Henry, B. and Silva, P. 2008. Multi-stage evolution of a sub-aerial volcanic ridge over the last 1.3 Myr: S. Jorge Island, Azores Triple Junction. *Earth Plan. Sci. Lett.*, **273**, 289-298, https://doi.org/10.1016/j.epsl.2008.06.041.

Hiscott, R., Colella, A., Pezard, P., Lovell, M. and Malinverno, A. 1992. Sedimentology of deep-water volcaniclastics, Oligocene Izu-Bonin forearc basin, based on formation microscanner images. *Proceedings of the Ocean Drilling Program, Scientific Results*, **126**, 75-96, https://doi.org/10.2973/odp.proc.sr.126.118.1992.

Hoogakker, B.A.A., Rothwell, R.G., Rohling, E.J., Paterne, M., Stow, D.A.V., Herrle, J.O. and Clayton, T. 2004. Variations in terrigenous dilution in western Mediterranean Sea pelagic sediments in response to climate change during the last glacial cycle. *Marine Geology*, **211**, 21-43, https://doi.org/10.1016/j.margeo.2004.07.005.

Houghton, B.F. and Landis, C.A. 1989. Sedimentation and volcanism in a Permian arc-related basin, southern New Zealand. *Bulletin of Volcanology*, **51**, 433-450, https://doi.org/10.1007/BF01078810.

Hunt, J.E., Wynn, R.B., Talling, P.J. and Masson, D.G. 2013. Multistage collapse of eight western Canary Island landslides in the last 1.5 Ma: Sedimentological and geochemical evidence from subunits in submarine flow deposits. *Geochemistry, Geophysics, Geosystems*, **14**, 2159-2181, https://doi.org/10.1002/ggge.20138.

Hunt, J.E., Wynn, R.B., Masson, D.G., Talling, P.J. and Teagle, D.A.H. 2011. Sedimentological and geochemical evidence for multistage failure of volcanic island landslides: A case study from Icod landslide on north Tenerife, Canary Islands. *Geochemistry, Geophysics, Geosystems*, **12**, https://doi.org/10.1029/2011gc003740.

Jarosewich, E. 2002. Smithsonian microbeam standards. *Journal of Research of the National Institute of Standards and Technology*, **107**, 681, https://doi.org/10.6028/jres.107.054.

Keating, B.H. and McGuire, W.J. 2000. Island edifice failure and associated tsunami hazards. *Pure Appl. Geophys.*, **157**, 899-955, https://doi.org/10.1007/s000240050011.

Keil, R.G., Montluçon, D.B., Prahl, F.G. and Hedges, J.I. 1994. Sorptive preservation of labile organic matter in marine sediments. *Nature*, **370**, 549-552, https://doi.org/10.1038/370549a0.

Kratzmann, D.J., Carey, S., Scasso, R. and Naranjo, J.-A. 2009. Compositional variations and magma mixing in the 1991 eruptions of Hudson volcano, Chile. *Bulletin of Volcanology*, **71**, 419, https://doi.org/10.1007/s00445-008-0234-x.

Krumbein, W.C. 1941. Measurement and geological significance of shape and roundness of sedimentary particles. *Journal of Sedimentary Research*, **11**, 64-72, https://doi.org/10.1306/D42690F3-2B26-11D7-8648000102C1865D.

Kutterolf, S., Freundt, A. and Burkert, C. 2011. Eruptive history and magmatic evolution of the 1.9 kyr Plinian dacitic Chiltepe Tephra from Apoyeque volcano in west-central Nicaragua. *Bulletin of Volcanology*, **73**, 811-831, https://doi.org/10.1007/s00445-011-0457-0.

Larrea, P., Wijbrans, J.R., Galé, C., Ubide, T., Lago, M., França, Z. and Widom, E. 2014. $^{40}Ar/^{39}Ar$ constraints on the temporal evolution of Graciosa Island, Azores (Portugal). *Bulletin of Volcanology*, **76**, 1-15, https://doi.org/10.1007/s00445-014-0796-8.

Le Friant, A., Harford, C.L., Deplus, C., Boudon, G., Sparks, R.S.J., Herd, R.A. and Komorowski, J.C. 2004. Geomorphological evolution of Montserrat (West Indies): importance of flank collapse and erosional process. *J. Geol. Soc. Lond.*, **161**, 147-160, https://doi.org/10.1144/0016-764903-017.

Le Friant, A., Ishizuka, O. *et al.* 2015. Submarine record of volcanic island construction and collapse in the Lesser Antilles arc: First scientific drilling of submarine volcanic island landslides by IODP Expedition 340. *Geochemistry, Geophysics, Geosystems*, **16**, 420-442, https://doi.org/10.1002/2014GC005652.

Lee, H.J., Torresan, M.E. and McArthur, W. 1994. Stability of submerged slopes on the flanks of the Hawaiian Islands, a simplified approach. *Open-File Report*, **94-638**, 1-54, https://doi.org/10.2172/90387.

Lourenço, N., Miranda, J.M., Luis, J.F., Ribeiro, A., Victor, L.A.M., Madeira, J. and Needham, H.D. 1998. Morpho-tectonic analysis of the Azores volcanic plateau from a new bathymetric compilation of the area. *Marine Geophys. Res.*, **20**, 141-156, https://doi.org/10.1023/A:1004505401547.

Louvat, P. and Allègre, C.J. 1998. Riverine erosion rates on Sao Miguel volcanic island, Azores archipelago. *Chem. Geol.*, **148**, 177-200, https://doi.org/10.1016/S0009-2541(98)00028-X.

Lowe, D.J., Pearce, N.J.G., Jorgensen, M.A., Kuehn, S.C., Tryon, C.A. and Hayward, C.L. 2017. Correlating tephras and cryptotephras using glass compositional analyses and numerical and statistical methods: Review and evaluation. *Quaternary Science Reviews*, **175**, 1-44, https://doi.org/10.1016/j.quascirev.2017.08.003.

Machado, F. 1959. Submarine pits of the azores plateau. *Bulletin Volcanologique*, **21**, 109-116, https://doi.org/10.1007/BF02596510.

Madeira, J. 1998. *Estudos de neotectónica nas ilhas do Faial, Pico e S. Jorge: uma contribuição para o conhecimento geodinâmico da junção tripla dos Açores.* Ph.D. dissertation, Lisbon University.

Madeira, J. and Brum da Silveira, A. 2003. Active tectonics and first paleoseismological results in Faial, Pico and S. Jorge islands (Azores, Portugal). *Annals of Geophys.*, **46**, 733-761, https://doi.org/10.4401/ag-3453.

Manga, M., Patel, A. and Dufek, J. 2011. Rounding of pumice clasts during transport: field measurements and laboratory studies. *Bulletin of Volcanology*, **73**, 321-333, https://doi.org/doi:10.1007/s00445-010-0411-6.

Marques, F.O., Hildenbrand, A. and Hübscher, C. 2018. Evolution of a volcanic island on the shoulder of an oceanic rift and geodynamic implications: S. Jorge Island on the Terceira Rift, Azores Triple Junction. *Tectonophysics*, **738-739**, 41-50, https://doi.org/10.1016/j.tecto.2018.05.012.

Martin, J.H., Knauer, G.A., Karl, D.M. and Broenkow, W.W. 1987. VERTEX: carbon cycling in the northeast Pacific. *Deep Sea Research Part A. Oceanographic Research Papers*, **34**, 267-285, https://doi.org/10.1016/0198-0149(87)90086-0.

Masson, D.G., Harbitz, C.B., Wynn, R.B., Pedersen, G. and Lovholt, F. 2006. Submarine landslides: processes, triggers and hazard prediction. *Phil. Trans Roy. Soc.*, **A364**, 2009-2039, https://doi.org/10.1098/rsta.2006.1810.

Menard, H.W. 1983. Insular erosion, isostasy, and subsidence. *Science*, **220**, 913-918, https://doi.org/10.1126/science.220.4600.913.

Meyers, P.A. 1994. Preservation of elemental and isotopic source identification of sedimentary organic matter. *Chem. Geol.*, **114**, 289-302, https://doi.org/10.1016/0009-2541(94)90059-0.

Miranda, J.M., Luis, J.F., Lourenço, N. and Fernandes, R.M.S. 2015. The structure and evolution of the Azores Triple Junction: implications for S. Miguel Island. *In*: Gaspar, J.L., Guest, J.E., Duncan, A.M., Barriga, F.J.A. and Chester, D.K. (eds) *Volcanic Geology of São Miguel Island (Azores Archipelago)*. Geol. Soc., Lond., London, 5-13, https://doi.org/10.1144/M44.2.

Mitchell, N.C., Dade, W.B. and Masson, D.G. 2003. Erosion of the submarine flanks of the Canary Islands. *J. Geophys. Res.*, **108**, https://doi.org/10.1029/2002JF000003.

Mitchell, N.C., Stretch, R., Tempera, F. and M., L. 2018. Volcanism in the Azores: A marine geophysical perspective. *In*: Beier, C. and Küppers, U. (eds) *Volcanoes of the Azores*. Springer, Berlin, Heidelberg, https://doi.org/10.1007/978-3-642-32226-6_7.

Mitchell, N.C., Beier, C., Rosin, P., Quartau, R. and Tempera, F. 2008. Lava penetrating water: Submarine lava flows around the coasts of Pico Island, Azores. *Geochemistry, Geophysics, Geosystems*, **9**, Paper Q03024, https://doi.org/10.1029/2007GC001725.

Moore, J.G., Normark, W.R. and Holcomb, R.T. 1994. Giant Hawaiian landslides. *An. Rev. Earth. Planet. Sci.*, **22**, 119-144, https://doi.org/10.1146/annurev.ea.22.050194.001003.

Nunes, J.C. 1999. *A actividade vulcânica na Ilha do Pico do Plistocénico Superior ao Holocénico: Mecanismo eruptivo e hazard vulcânico.* PhD, Universidade dos Acores.

Ollier, G., Cochonat, P., Lenat, J.F. and Labazuy, P. 1998. Deep-sea volcaniclastic sedimentary systems: an example from La Fournaise volcano, Reunion Island, Indian Ocean. *Sedimentology*, **45**, 293-330, https://doi.org/10.1046/j.1365-3091.1998.0152e.x.

Pacheco, J. 2002. Processos associados ao desenvolvimento de erupções vulcânicas hidromagmáticas explosivas na ilha do Faial e sua interpretação numa perspectiva de avaliação do hazard e minimização do risco.

Pimentel, A., Pacheco, J. and Self, S. 2015. The~ 1000-years BP explosive eruption of Caldeira Volcano (Faial, Azores): the first stage of incremental caldera formation. *Bulletin of Volcanology*, **77**, 1-26, https://doi.org/10.1007/s00445-015-0930-2.

Pimentel, A.H.G. 2007. *Domos e coulées da ilha Terceira (Açores): contribuição para o estudo dos mecanismos de instalação.* MSc dissertation, Universidade dos Açores.

Quartau, R., Trenhaile, A.S., Mitchell, N.C. and Tempera, F. 2010. Development of volcanic insular shelves: Insights from observations and modelling of Faial Island in the Azores Archipelago. *Marine Geology*, **275**, 66-83, https://doi.org/10.1016/j.margeo.2010.04.008.

Quartau, R., Madeira, J., Mitchell, N.C., Tempera, F., Silva, P.F. and Brandão, F. 2015. The insular shelves of the Faial-Pico Ridge (Azores archipelago): A morphological record of its evolution. *Geochemistry, Geophysics, Geosystems*, **16**, 1401-1420, https://doi.org/10.1002/2015GC005733.

Quartau, R., Tempera, F. *et al.* 2012. Morphology of Faial Island's shelf: The results of volcanic, erosional, depositional and mass-wasting processes. *Geochemistry, Geophysics, Geosystems*, **13**, https://doi.org/10.1029/2011GC003987.

Reid, R., Carey, S.N. and Ross, D.R. 1996. Late Quaternary sedimentation in the Lesser Antilles island arc. *Geol. Soc. Am. Bull,*, **108**, 78-100, https://doi.org/10.1130/0016-7606(1996)108<0078:LQSITL>2.3.CO;2.

Saint-Ange, F., Bachèlery, P., Babonneau, N., Michon, L. and Jorry, S.J. 2013. Volcaniclastic sedimentation on the submarine slopes of a basaltic hotspot volcano: Piton de la Fournaise volcano (La Réunion Island, Indian Ocean). *Marine Geology*, **337**, 35-52, https://doi.org/10.1016/j.margeo.2013.01.004.

Savrda, C.E., Krawinkel, H., McCarthy, F.M.G., McHugh, C.M.G., Olson, H.C. and Mountain, G. 2001. Ichnofabrics of a Pleistocene slope succession, New Jersey margin: relations to climate and sea-level dynamics. *Palaeogeography, Palaeoclimatology, Palaeoecology*, **171**, 41-61, https://doi.org/10.1016/S0031-0182(01)00266-8.

Schindlbeck, J.C., Kutterolf, S., Freundt, A., Scudder, R.P., Pickering, K.T. and Murray, R.W. 2013. Emplacement processes of submarine volcaniclastic deposits (IODP Site C0011, Nankai Trough). *Marine Geology*, **343**, 115-124, https://doi.org/10.1016/j.margeo.2013.06.017.

Schlager, W. 2000. Sedimentation rates and growth potential of tropical, cool-water and mud-mound carbonate systems. *Geological Society, London, Special Publications*, **178**, 217-227, https://doi.org/10.1144/GSL.SP.2000.178.01.14.

Schmincke, H.-U. and Sumita, M. 1998. Tephra event stratigraphy and emplacement of volcaniclastic sediments, Mogán and Fataga stratigraphic intervals, Part II: origin and emplacement of volcaniclastic layers. *Proc. ODP, Sci. Results*, **157**, 267-291, https://doi.org/10.2973/odp.proc.sr.157.113.1998.

Schneider, J.-L., Le Ruyet, A., Chanier, F., Buret, C., Ferrière, J., Proust, J.-N. and Rosseel, J.-B. 2001. Primary or secondary distal volcaniclastic turbidites: how to make the distinction? An example from the Miocene of New Zealand (Mahia Peninsula, North Island). *Sedimentary Geology*, **145**, 1-22, https://doi.org/10.1016/S0037-0738(01)00108-7.

Schultz, L.G. 1964. Quantitative interpretation of mineralogical composition from X-ray and chemical data for the Pierre Shale. *Professional Paper*, https://doi.org/10.3133/pp391C.

Scudder, R.P., Murray, R.W. *et al.* 2016. Geochemical approaches to the quantification of dispersed volcanic ash in marine sediment. *Progress in Earth and Planetary Science*, **3**, 1, https://doi.org/10.1186/s40645-015-0077-y.

Self, S. 1976. The recent volcanology of Terceira, Azores. *J. Geol. Soc. Lond.*, **132**, 645-666, https://doi.org/10.1144/gsjgs.132.6.0645.

Sibrant, A.L.R., Marques, F.O. and Hildenbrand, A. 2014. Construction and destruction of a volcanic island developed inside an oceanic rift: Graciosa Island, Terceira Rift, Azores. *J. Volcanol. Geother. Res.*, **284**, 32-45, https://doi.org/10.1016/j.jvolgeores.2014.07.014.

Sigurdsson, H. and Sparks, R. 1981. Petrology of rhyolitic and mixed magma ejecta from the 1875 eruption of Askja, Iceland. *Jour. Petrol.*, **22**, 41-84, https://doi.org/10.1093/petrology/22.1.41.

Sigurdsson, H., Sparks, R., Carey, S.t. and Huang, T. 1980. Volcanogenic sedimentation in the Lesser Antilles arc. *The Journal of Geology*, **88**, 523-540, https://doi.org/10.1086/628542.

Sigurdsson, H., Kelley, S., Leckie, R., Carey, S., Bralower, T. and King, J. 2000. 20: History of circum-Caribbean explosive volcanism: $^{40}Ar/^{39}Ar$ dating of tephra layers. *Proceedings of the Ocean Drilling Program, Scientific Results. College Station TX, Texas A&M*, 299-314, https://doi.org/10.2973/odp.proc.sr.165.021.2000.

Solaro, C., Boudon, G., Le Friant, A., Balcone-Boissard, H., Emmanuel, L. and Paterne, M. 2020. New insights into the recent eruptive and collapse history of Montagne Pelée (Lesser Antilles Arc) from offshore marine drilling site U1401A (IODP Expedition 340). *J. Volcanol. Geother. Res.*, **403**, 107001, https://doi.org/10.1016/j.jvolgeores.2020.107001.

Stokes, S. and Lowe, D.J. 1988. Discriminant function analysis of late Quaternary tephras from five volcanoes in New Zealand using glass shard major element chemistry. *Quat. Res.*, **30**, 270-283, https://doi.org/10.1016/0033-5894(88)90003-8.

Stokes, S., Lowe, D.J. and Froggatt, P.C. 1992. Discriminant function analysis and correlation of Late Quaternary rhyolitic tephra deposits from Taupo and Okataina volcanoes, New Zealand, using glass shard major element composition. *Quaternary International*, **13-14**, 103-117, https://doi.org/10.1016/1040-6182(92)90016-U.

Stow, D.A.V. and Piper, D.J.W. 1984. Deep-water fine-grained sediments: facies models. *Geological Society, London, Special Publications*, **15**, 611-646, https://doi.org/10.1144/gsl.Sp.1984.015.01.38.

Talling, P.J. 2001. On the frequency distribution of turbidite thickness. *Sedimentology*, **48**, 1297-1329, https://doi.org/10.1046/j.1365-3091.2001.00423.x.

Talling, P.J., Masson, D.G., Sumner, E.J. and Malgesini, G. 2012. Subaqueous sediment density flows: Depositional processes and deposit types. *Sedimentology*, **59**, 1937-2003, https://doi.org/10.1111/j.1365-3091.2012.01353.x.

Trofimovs, J., Sparks, R.S.J. and Talling, P.J. 2008. Anatomy of a submarine pyroclastic flow and associated turbidity current: July 2003 dome collapse, Soufrière Hills volcano, Montserrat, West Indies. *Sedimentology*, **55**, 617-634, https://doi.org/10.1111/j.1365-3091.2007.00914.x.

Trofimovs, J., Amy, L. *et al.* 2006. Submarine pyroclastic deposits formed at the Soufrière Hills volcano, Montserrat (1995 -2003): What happens when pyroclastic flows enter the ocean? *Geology*, **34**, 549-552, https://doi.org/10.1130/G22424.1.

Trofimovs, J., Talling, P.J. *et al.* 2013. Timing, origin and emplacement dynamics of mass flows offshore of SE Montserrat in the last 110 ka: Implications for landslide and tsunami hazards, eruption history, and volcanic island evolution. *Geochemistry, Geophysics, Geosystems*, **14**, 385-406, https://doi.org/10.1002/ggge.20052.

Valente, E.M.L. 2020. *Sedimentary dynamics on insular shelves of volcanic islands: insights from two marine cores of Faial shelf, Azores.* Master thesis, Universidade de Lisboa

van Andel, T.H. and Komar, P.D. 1969. Ponded sediments of the Mid-Atlantic Ridge between 22˚ and 23˚ North latitude. *Geol. Soc. Am. Bull.*, **80**, 1163-1190, https://doi.org/10.1130/0016-7606(1969)80[1163:PSOTMR]2.0.CO;2.

Vlag, P.A., Kruiver, P.P. and Dekkers, M.J. 2004. Evaluating climate change by multivariate statistical techniques on magnetic and chemical properties of marine sediments (Azores region). *Palaeogeography, Palaeoclimatology, Palaeoecology*, **212**, 23-44, https://doi.org/10.1016/j.palaeo.2004.05.015.

Vogt, P.R. and Jung, W.Y. 2004. The Terceira Rift as a hyper-slow, hotspot-dominated oblique spreading axis: A comparison with other slow-spreading plate boundaries. *Earth and Planet. Sci. Letts.*, **218**, 77-90, https://doi.org/10.1016/S0012-821X(03)00627-7.

Walker, G.P.L. 1981. Generation and dispersal of fine ash and dust by volcanic eruptions. *J. Volcanol. Geother. Res.*, **11**, 81-92, https://doi.org/10.1016/0377-0273(81)90077-9.

Walker, R.G. 1978. Deep-water sandstone facies and ancient submarine fans: models for exploration for stratigraphic traps. *AAPG bulletin*, **62**, 932-966, https://doi.org/10.1306/C1EA4F77-16C9-11D7-8645000102C1865D.

Wall-Palmer, D., Coussens, M. *et al.* 2014. Late Pleistocene stratigraphy of IODP Site U1396 and compiled chronology offshore of south and south west Montserrat, Lesser Antilles. *Geochemistry, Geophysics, Geosystems*, **15**, 3000-3020, https://doi.org/10.1002/2014GC005402.

Weston, F.S. 1964. *A list of recorded volcanic eruptions in the Azores with brief reports.* 10 (1), Universidade de Lisboa.

Wetzel, A. and Uchman, A. 2012. Chapter 22 - Hemipelagic and Pelagic Basin Plains. *In*: Knaust, D. and Bromley, R.G. (eds) *Developments in Sedimentology*. Elsevier, 673-701, https://doi.org/10.1016/B978-0-444-53813-0.00022-8.

White, W., Schilling, J.-G. and Hart, S. 1976. Evidence for the Azores mantle plume from strontium isotope geochemistry of the Central North Atlantic. *Nature*, **263**, 659-663, https://doi.org/10.1038/263659a0.

Whitham, A.G. 1989. The behaviour of subaerially produced pyroclastic flows in a subaqueous environment: Evidence from the Roseau eruption, Dominica, West Indies. *Marine Geology*, **86**, 27-40, https://doi.org/10.1016/0025-3227(89)90016-9.

Wilson, C.J. and Hildreth, W. 1998. Hybrid fall deposits in the Bishop Tuff, California: A novel pyroclastic depositional mechanism. *Geology*, **26**, 7-10, https://doi.org/10.1130/0091-7613(1998)026<0007:HFDITB>2.3.CO;2.

Wisshak, M., Form, A., Jakobsen, J. and Freiwald, A. 2010. Temperate carbonate cycling and water mass properties from intertidal to bathyal depths (Azores). *Biogeosciences*, **7**, 2379-2396, https://doi.org/10.5194/bg-7-2379-2010.

Wisshak, M., Berning, B., Jakobsen, J. and Freiwald, A. 2015. Temperate carbonate production: biodiversity of calcareous epiliths from intertidal to bathyal depths (Azores). *Marine Biodiversity*, **45**, 87-112, https://doi.org/10.1007/s12526-014-0231-6.

Woodhall, D. 1974. Geology and volcanic history of Pico Island Volcano, Azores. *Nature*, **248**, 663-665, https://doi.org/10.1038/248663a0.

Zbyszewski, G., Candido de Mederos, A., da Veiga Ferreira, O., Rodrigues, L. and Rodrigues, A. 1974. *Carta geologica de Portugal: Ilha da Madeira B*.

Zhao, Z., Mitchell, N.C., Quartau, R., Tempera, F. and Bricheno, L. 2019. Submarine platform development by erosion of a Surtseyan cone at Capelinhos, Faial Island, Azores. *Earth surface proc. landforms*, **44**, 2982-3006, https://doi.org/doi:10.1002/esp.4724.

Zhao, Z., Mitchell, N.C., Quartau, R., Ramalho, R.S. and Rusu, L. 2020. Coastal erosion rates of lava deltas around oceanic islands. *Geomorphology*, **370**, 107410, https://doi.org/10.1016/j.geomorph.2020.107410.

1071 Table

1072 Table 1

Facies classification	Facies 1 Clay-rich hemipelagic mud	Facies 2a Carbonate-rich and clay-poor volcaniclastic deposits	Facies 2b Carbonate-poor and clay-poor volcaniclastic deposits
Lithology	Ungraded mud	1.Silt to pebble 2.Light-coloured sediments intercalated in the black sediments	1.Silt to pebble 2.Silt to coarse sand
Abundance of microfossils	Some and evenly distributed	1.Many but usually fragmented 2.Many	1.Few 2.Few
Sedimentary structures	Generally homogeneous mud. Dispersed burrows and mottled structures are common. Volcanic clast pods are occasionally found	1.Sharp scouring surface on the bottom. Apparent normal graded bedding with parallel laminations in the coarse grains. 2.Burrows, and inconsistent laminations	1.Sharp scouring surface at base; usually normal graded beddings, occasionally with inverse graded bedding in the middle 2.Normally graded. Often with bioturbated top
Bed lower boundary	Gradational change	1.Sharp erosive contact 2.Chaotic surface	1.Sharply erosive contact 2.Sharp contact occasionally with tephra intrusion into the lower bedding
Colours	Pale brown or pale grey occasionally with dispersed dark mottles in between	1.light to dark brown base with scattered white dots 2.Dark and light sediments unevenly mixed	1.Generally dark yet gradually lighter upward 2.Generally dark yet gradually lighter upward
Geochemical composition of volcanic glass	Mostly heterogeneous	1.Usually heterogeneous 2.Homogeneous and heterogeneous are possible	1.Usually homogenous 2.Homogeneous
Angularity of volcanic grains	Typically rounded, near-spherical	1.Typically rounded and near-spherical 2.Rounded and angular are possible.	1.Rounded and angular are possible. 2.Angular
Depositional process	Sediment slowly and progressively settled on seabed	1.Volcaniclastic turbidity currents incorporating shelf or slope carbonate material. 2.Intense bioturbation after volcaniclastic deposits were emplaced	1.Volcaniclastic turbidity currents with minor or without carbonate incorporated from shelf or slope. 2.Air fallout
Interpretation	Background sedimentation	1.Can be either primary or secondary event 2.Can be either primary or secondary event	1.Mostly primary event and rarely secondary event 2.Primary fallout

1073 *Numbers in facies 2a and 2b columns associate aspects of the facies that were used to
1074 interpret the emplacement mechanisms.

1075

1076 Figures

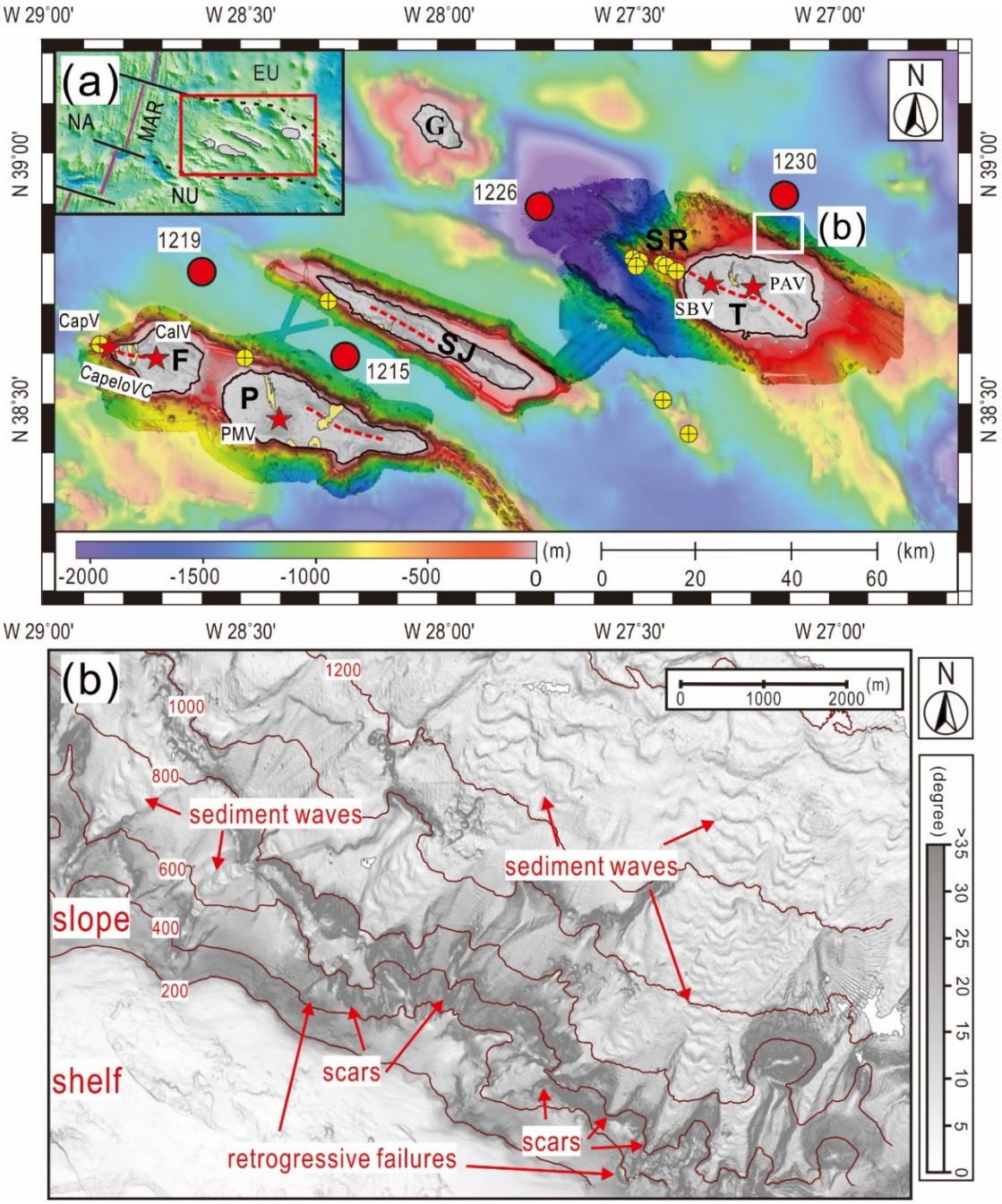

1077

1078 **Fig. 1**. (a) Locations of the four investigated gravity cores (numbered red circles) between the
1079 five central Azores Islands (shown in grey with black outlines) of Faial (F), Pico (P), São Jorge
1080 (SJ), Graciosa (G), and Terceira (T) with the submarine Serreta Ridge (SR). Red stars and
1081 dotted lines are recently or presently on-land active volcanoes and fissure zones or cinder cone
1082 alignments. Volcanoes active in late Pleistocene and Holocene times are, from the west to east,
1083 Capelinhos volcano (CapV), Capelo Volcanic Complex (CapeloVC), Caldeira (CalV), Pico
1084 Mountain Volcano (PMV), Santa Bárbara Volcano (SBV), and Pico Alto Volcano (PAV).
1085 Yellow areas on land represent historical lava flows (Madeira 1998; Gaspar, 2003; Pimentel et
1086 al., 2016). Yellow crossed circles locate submarine eruption sites (Machado 1959; Weston
1087 1964; Queiroz et al. 1995; Gaspar et al., 2015). Background bathymetry is from the Global
1088 Multi-Resolution Topography synthesis (GMRT; Ryan et al., 2009); higher-resolution
1089 foreground bathymetry (bold colours) is from surveys in 2003 (Mitchell et al., 2008) and 2011

(Chiocci et al., 2013). Upper-left inset: location of the central Azores Islands in the diffuse boundary between the Eurasia (EU) and Nubia (NU) plates. NA: North American plate. Purple lines locate the Mid-Atlantic Ridge (MAR). Solid black lines locate fracture zones near the Mid-Atlantic Ridge and dashed black lines outline the diffuse NU-EU plate boundary (Laughton and Whitmarsh, 1974; Lourenço et al.,1998). (b) Enlarged map of local gradients on the north flank of Terceira revealing morphological features of the submarine slope. Depth contours in 200 m. Map located by white rectangle in (a). The source of map is from surveys in 2011 (Chiocci et al., 2013).

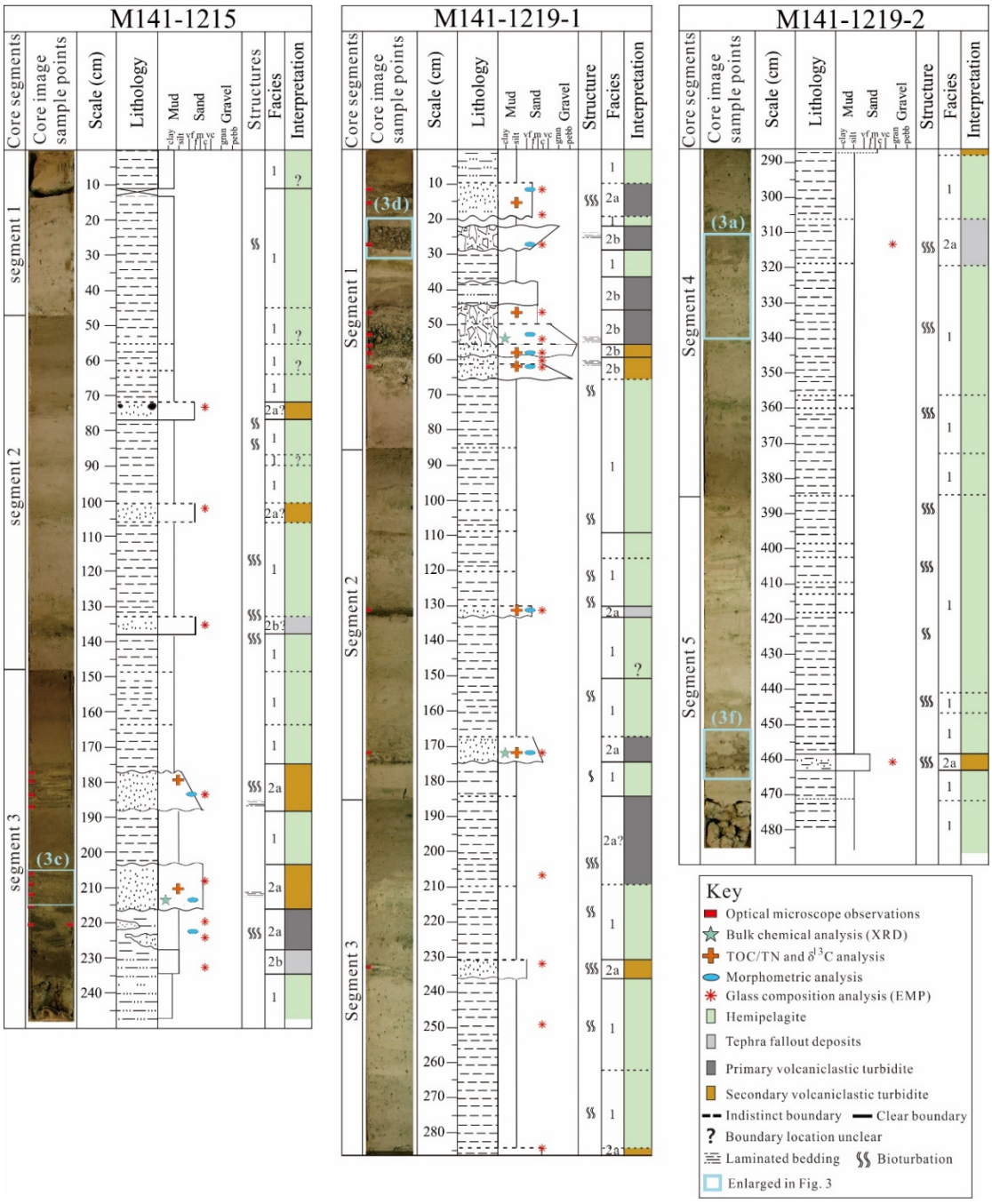

Fig. 2. Photographic scans, interpreted lithological columns, grain size with locations of analysed samples, sedimentary structures, and facies interpretations of the cores located in Fig. 1. The interpreted changes in overall grain size and abundance of microfossils were based on reflecting microscope observations.

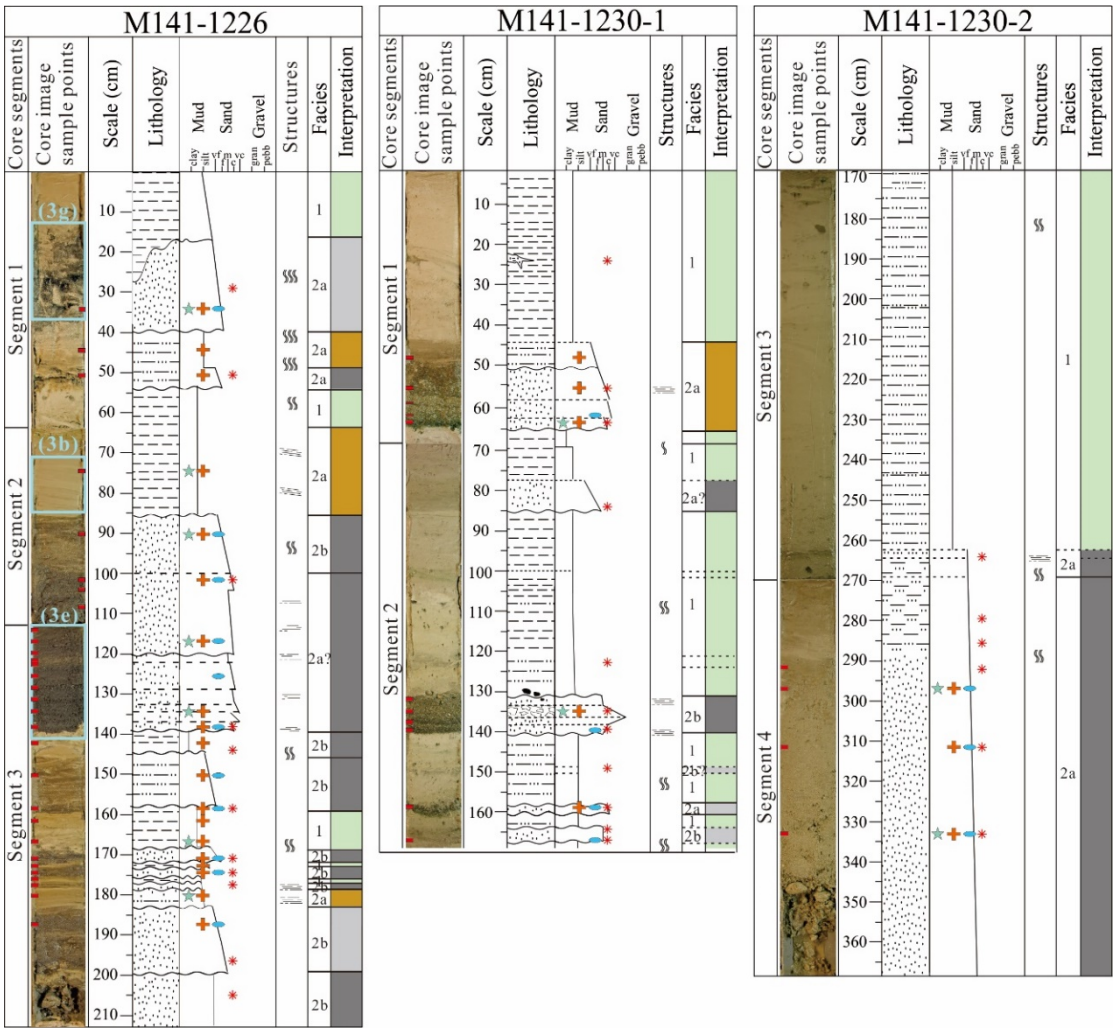

Fig. 2. Continued

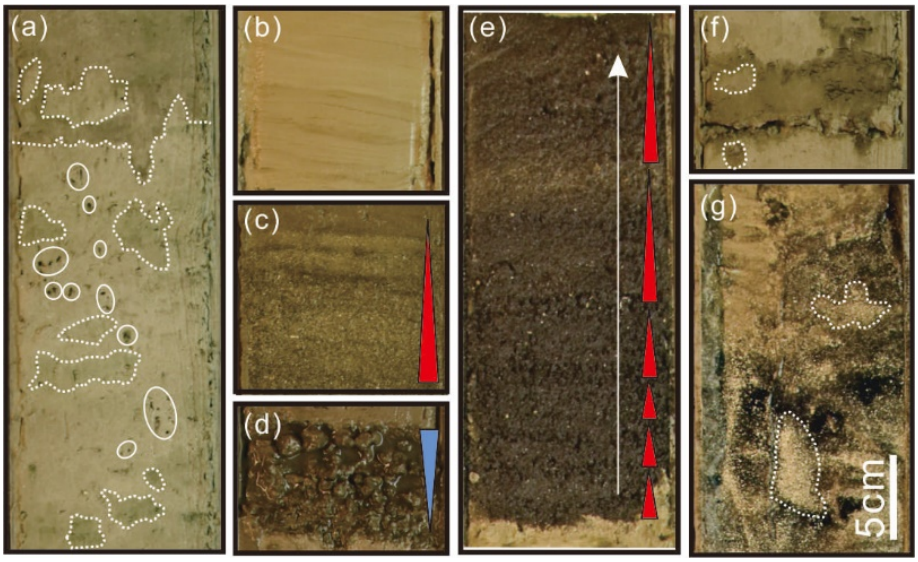

Fig. 3. Enlargements of core sections located by light blue rectangles in Fig. 2 illustrating sedimentary structures in each facies. (**a**) Bioturbated burrows in F1 (outlined by white dotted lines). Mafic grains dispersed by bioturbation are marked by white ellipses. (**b**) Gently dipping ripple marks in F2a. (**c**) Parallel laminations and normally graded bedding (red triangle). (**d**) Inverse-graded bedding (blue triangle) in F2b with scoured underlying surface. (e) An upward

fining sequence (white arrow) in F2b comprising multiple normally graded beds (red triangles) with sharp underlying boundary. (**f**) Burrows in a secondary turbidite of F2a. (**g**) Features caused by intense bioturbation, which have led to incorporation of carbonate in otherwise carbonate-poor volcaniclastic deposits. The distance scale shown is common to all photos.

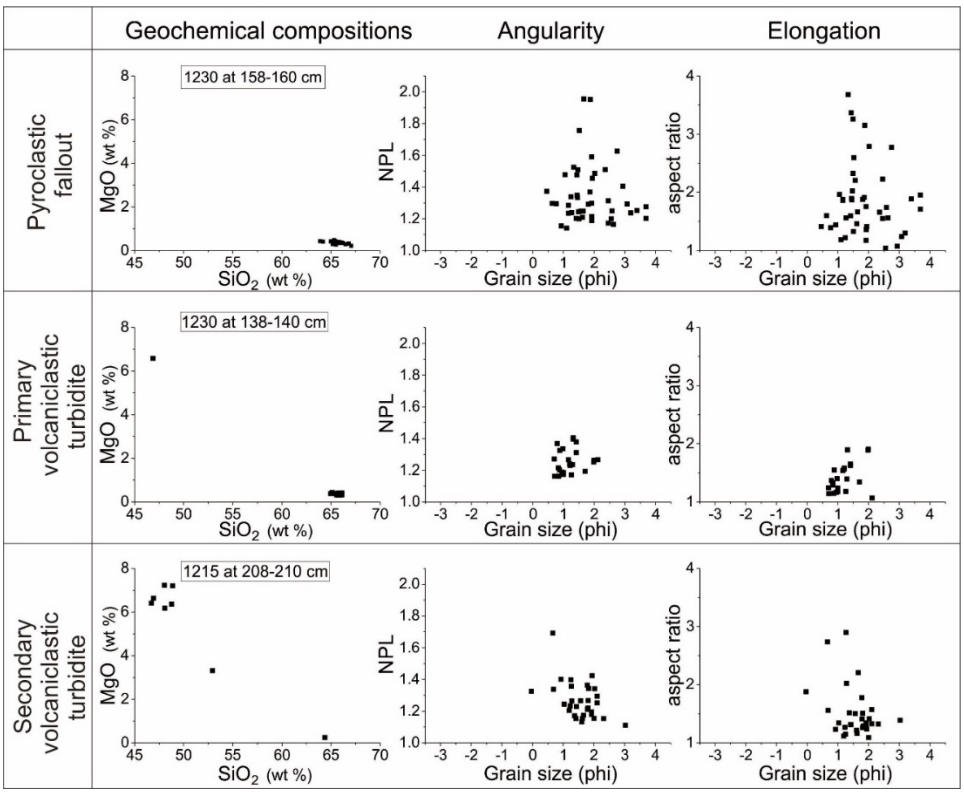

Fig. 4. Geochemical (left panels) and morphometric characteristics of volcanic particles from selected beds representing the three deposit types found in facies F2. NPL: normalized perimeter length. Diagrams for all analyzed beds can be found in supplement.

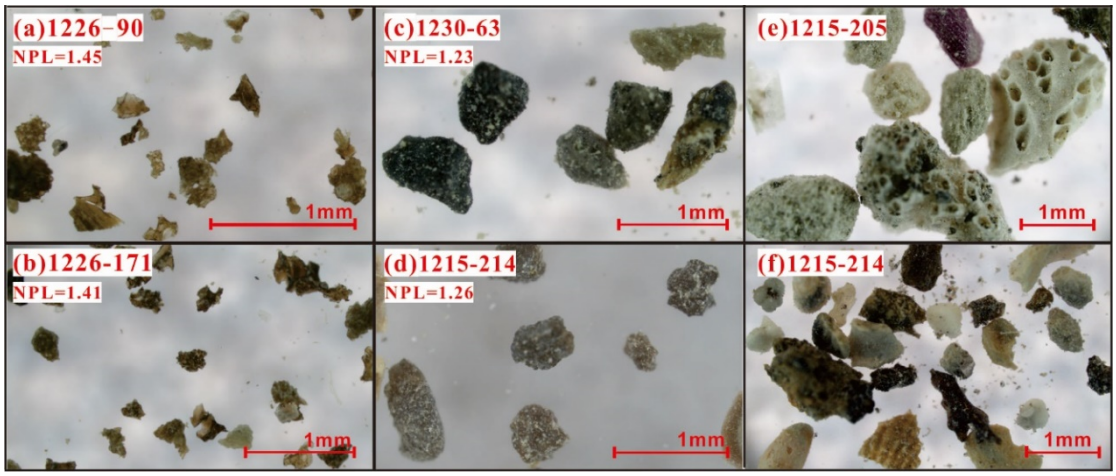

Fig. 5. Selected photos (reflected light) of volcanic particles and bioclasts from different core samples. Samples are located in Figure 2. (**a, b**): photos of angular vitric glass fragments from core 1226 at 90 and 173 cm. (**c, d**): photos of rounded volcanic clasts from core 1230 at 63 cm and core 1215 at 214 cm. (**e, f**): photos of coralline algae debris from core 1215 at 205 cm and foraminifera and shell fragments from core 1215 at 214 cm. All particles are from facies F2. NPL values were given in the photos of volcanic particles samples.

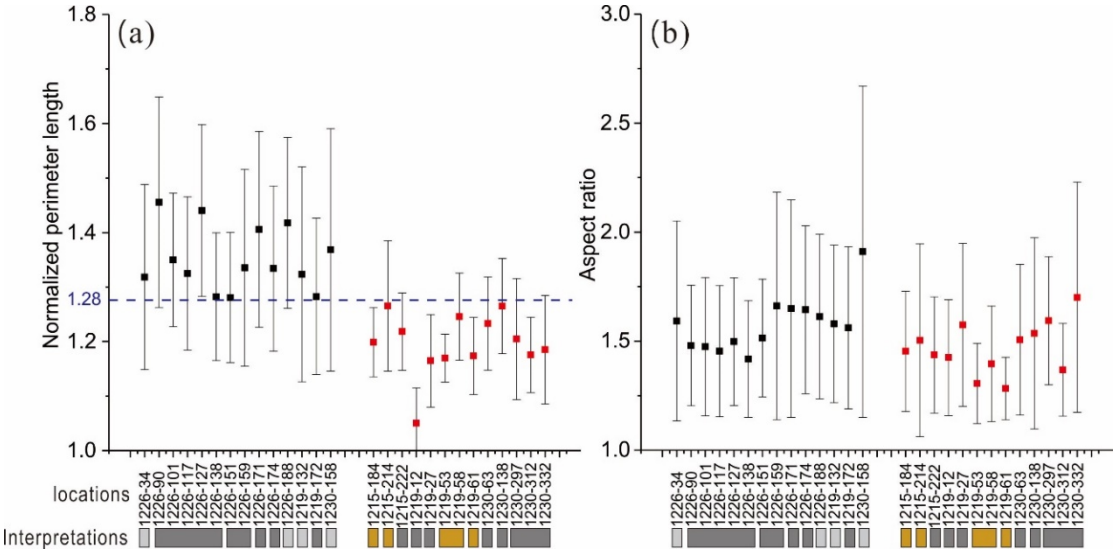

Fig. 6. Average values (solid squares) and one standard deviations (bars) of (**a**) normalized perimeter length and (**b**) aspect ratios of samples located in Fig. 2. Colours of rectangles below the graphs correspond with the right-most interpretation panels in Fig. 2. Rectangles crossing multiple samples are taken from the same bed but different locations. The data have been sorted into two groups with NPL>1.28 (black symbols) and NPL<1.28 (red symbols), which are interpreted as having without (black) and with (red) intense abrasion.

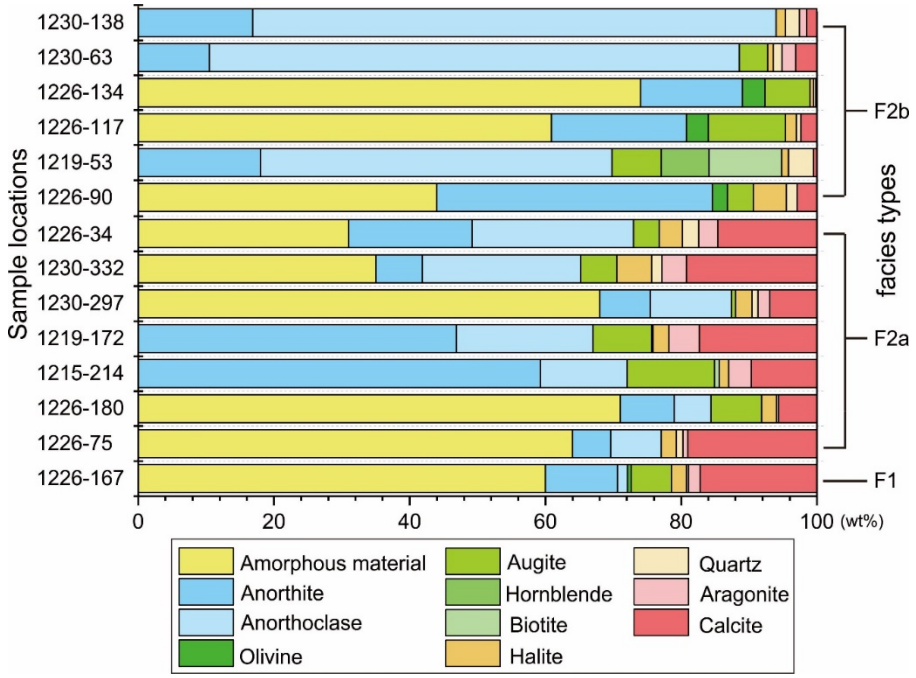

Fig. 7. Mineral assemblages from XRD analyses of bulk sediment samples. Yellow bars represent amorphous material. The two blue bars represent feldspars. The four green bars represent ferromagnesian minerals. The red and pink bars represent carbonate minerals.

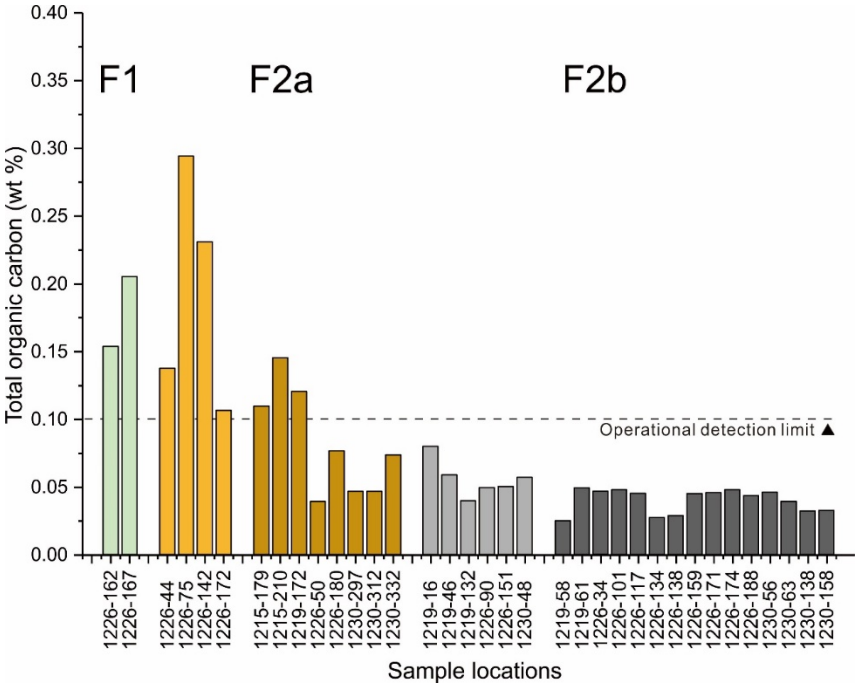

Fig. 8. Organic carbon contents of the samples located in Figure 2 sorted by facies. The light and dark tones of the colour bars are used to represent fine- and coarse-grained sediments of F2a and F2b. The 0.1 wt.% operational detection limit is marked.

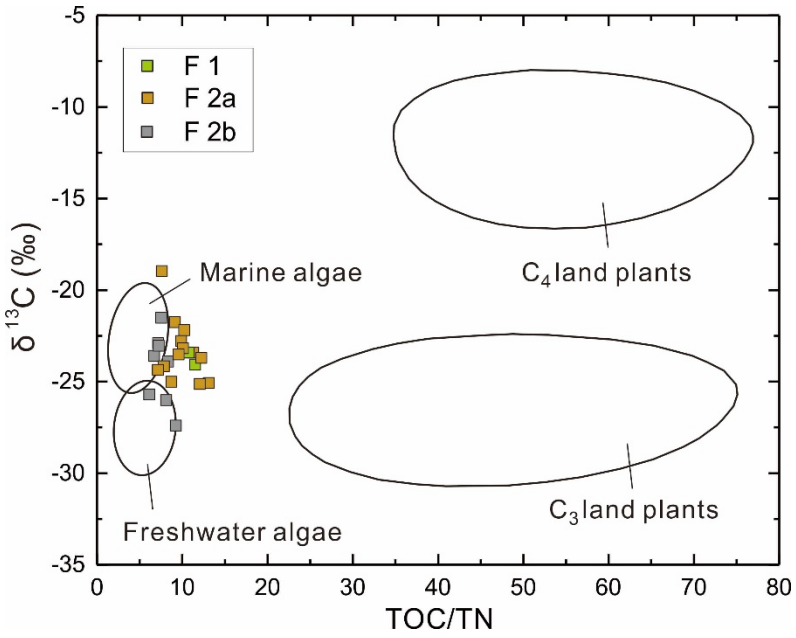

Fig. 9. $\delta^{13}C$ and ratios of total organic carbon and total nitrogen for the samples located in Figure 2. Reference data fields (ellipses) after Meyers (1994).

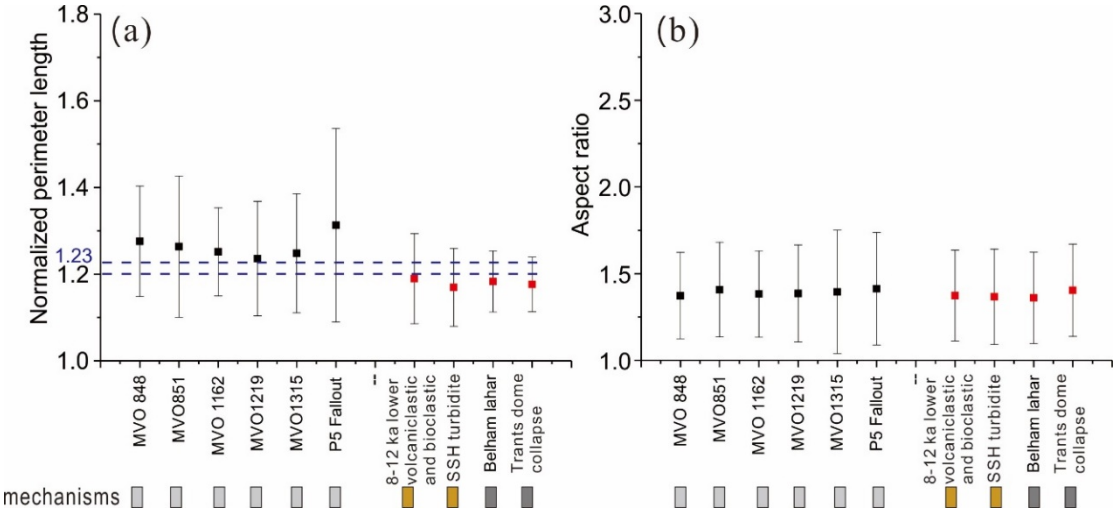

Fig. 10. Average values (solid squares) and one standard deviations (bars) of (a) normalized perimeter length and (b) aspect ratios of volcaniclastic particles constructed in the same style as Fig. 6 from the data of Cassidy et al. (2014), where the transport process was known independently. Colours of rectangles below the graphs correspond with the key in Fig. 2. The data have been sorted into pyroclastic fallout (black squares) and primary and secondary volcaniclastic turbidite (red squares) in each panel. Pyroclastic fallout has NPL>1.23 and without intense abrasion (black symbols). Turbidite instead has NPL<1.2 with intense abrasion (red symbols).

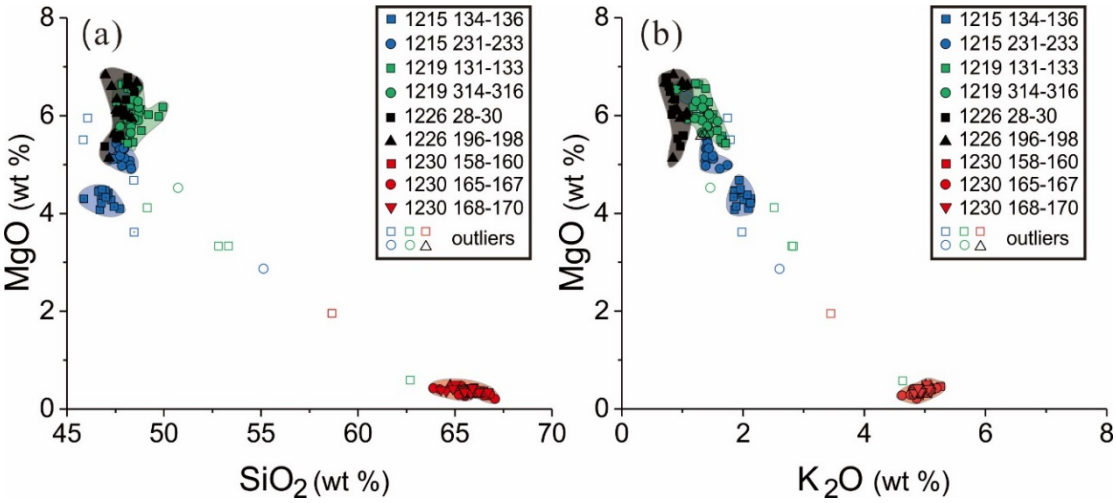

Fig. 11. Geochemical variations of volcanic glasses in selected samples interpreted as fallout. (a) MgO versus SiO_2. (b) MgO versus K_2O. Note that outliers have been left unfilled to avoid distraction from the clusters.

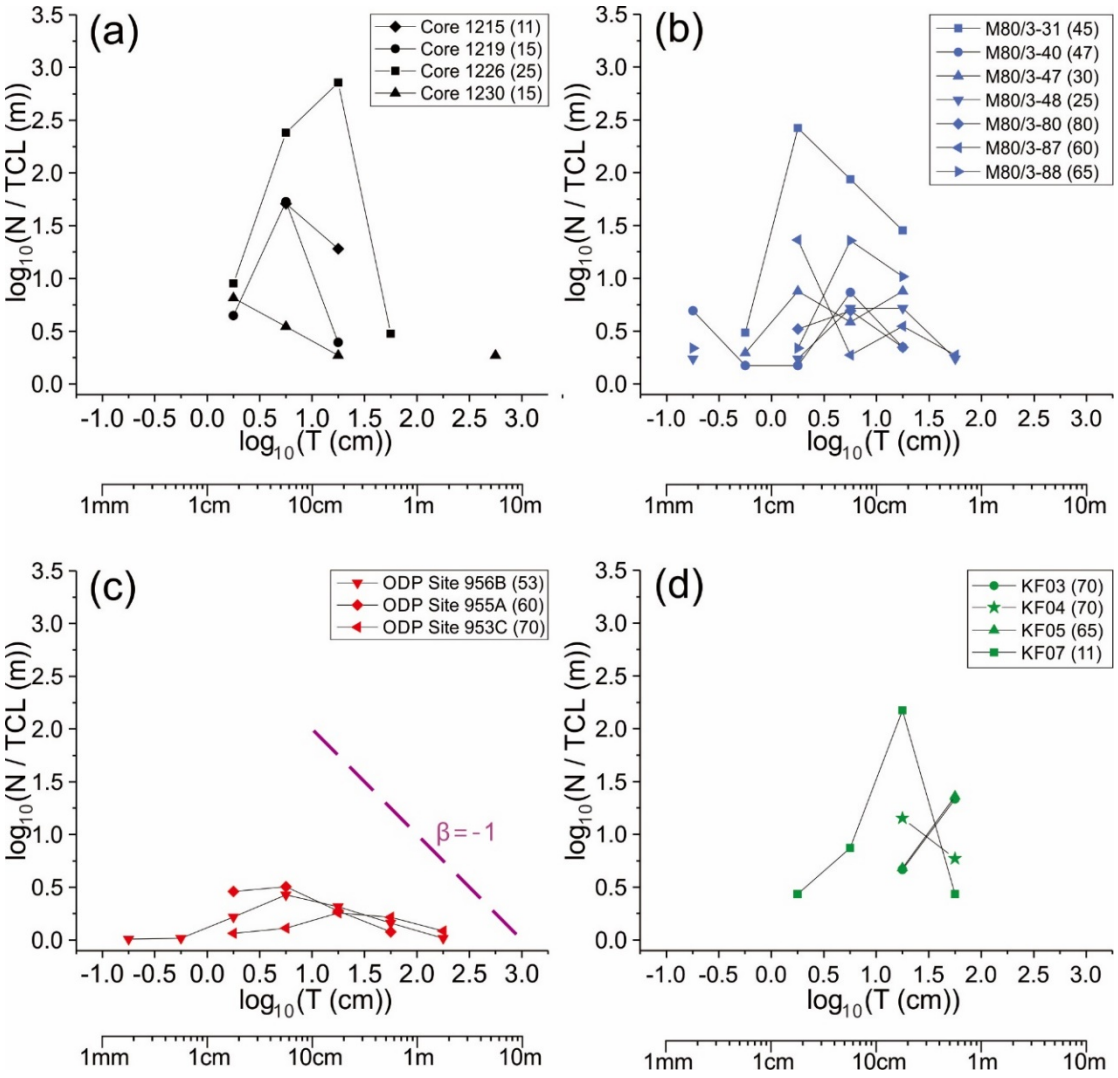

Fig. 12. Thickness frequency distributions of volcaniclastic beds preserved in comparatively proximal drilling sites of different volcanic settings (a) the central Azores (b) Cape Verde (c) Gran Canaria and (d) Reunion island. Counts of volcaniclastic beds (N) divided by total core length (TCL) are plotted against volcaniclastic bed thickness (T). The distances of cores to the coasts (km) are noted in the legends after the core sites. Note that both axes are logarithmic. The purple dashed line represents a graph-gradient of $\beta = -1$, which is similar to that found for volcaniclastic beds in the Izu-Bonin cores (Hiscott et al., 1992).